Computer Physics Communications 284 (2023) 108598

Contents lists available at ScienceDirect

Computer Physics Communications

journal homepage: www.elsevier.com/locate/cpc

PULSEE: A software for the quantum simulation of an extensive set of magnetic resonance observables ☆,☆☆

Davide Candoli [a,c,1], Ilija K. Nikolov [a], Lucas Z. Brito [a], Stephen Carr [a,b], Samuele Sanna [c], Vesna F. Mitrović [a,*]

[a] Department of Physics, Brown University, Providence, 02912 RI, USA
[b] Brown Theoretical Physics Center, Brown University, Providence, RI 02912-1843, USA
[c] Department of Physics and Astronomy "A. Righi", University of Bologna and INFN Sezione di Bologna, 40127 Bologna, Italy

ARTICLE INFO

Article history:
Received 1 August 2021
Received in revised form 1 November 2022
Accepted 13 November 2022
Available online 23 November 2022

Keywords:
Nuclear magnetic resonance
Nuclear quadrupole resonance
Quadrupolar interaction
Spin dynamics
Magnetic resonance
Quantum computing
Python 3

ABSTRACT

We present an open-source software for simulation of observables in magnetic resonance experiments, including nuclear magnetic/quadrupole resonance NMR/NQR and electron spin resonance (ESR). Inspired by magnetic resonance protocols that emerged in the context of quantum information science (QIS), this software can assist experimental research in the design of new strategies for the investigation of fundamental quantum properties of materials. The package introduced here can simulate both standard NMR spectroscopic observables and the time-evolution of an interacting single-spin system subject to complex pulse sequences, *i.e.* quantum gates. The main purpose of this software is to facilitate the development of much needed novel NMR-based probes of emergent quantum order, which can be elusive to standard experimental probes. The software is based on a quantum mechanical description of nuclear spin dynamics in NMR/NQR experiments and has been widely tested on available theoretical and experimental results. Moreover, the structure of the software allows for basic experiments to be easily generalized to more sophisticated ones because it includes all the libraries required for the numerical simulation of generic spin systems. In order to make the program easily accessible to a large user base, we developed a user-friendly graphical interface, Jupyter notebooks, and fully-detailed documentation. Lastly, we portray several examples of the execution of the code that illustrate the prosepcts of a novel NMR paradigm, inspired by QIS, for efficient investigation of emergent phases in strongly correlated materials.

Program summary

Program Title: PULSEE (Program for the simULation of nuclear Spin Ensemble Evolution)
CPC Library link to program files: https://doi.org/10.17632/vvv8tcb2nt.1
Developer's repository link: https://github.com/vemiBGH/PULSEE
Licensing provisions: GPLv3
Programming language: Python 3
Nature of problem: Application of nuclear magnetic/quadrupole resonance techniques to study properties of materials often requires extensive spectral simulations. On the other hand, application of magnetic resonance techniques to quantum information science (QIS) involves different sets of observables. Available simulation software addresses only one of these applications: either detailed spectral simulations [1] or QIS relevant observables [2]. For this reason, NMR has not seen as much development in the condensed matter community compared to other spectroscopic techniques that combine these two approaches. Therefore, there is a need for an up-to-date and easily accessible software that can simulate an extensive set of NMR/NQR experimental observables, reproducing the behavior/response of nuclear systems with a varying degree of complexity encountered in strongly correlated quantum materials.

☆ The review of this paper was arranged by Prof. Blum Volker.
☆☆ This paper and its associated computer program are available via the Computer Physics Communications homepage on ScienceDirect (http://www.sciencedirect.com/science/journal/00104655).

* Corresponding author.
E-mail address: vemi@brown.edu (V.F. Mitrović).
[1] Current affiliation - Institute for Quantum Optics and Quantum Information of the Austrian Academy of Sciences, A-6020 Innsbruck, Austria and Institute for Theoretical Physics, University of Innsbruck, A-6020 Innsbruck, Austria.

https://doi.org/10.1016/j.cpc.2022.108598

Solution method: The open-source Python code provides an extensive set of libraries for the simulation of spin time evolution in the presence of specific interactions and reproduction of spectra; as well as other observables measured in magnetic resonance experiments; and simulations of quantum circuits and gates. The ready-to-use software features a user-friendly graphical interface, and Jupyter notebooks.

References

[1] F. A. Perras, C. M. Widdifield, and D. L. Bryce, "*QUEST - Quadrupolar Exact Software: A fast graphical program for the exact simulation of NMR and NQR spectra for quadrupolar nuclei*," Solid State Nuclear Magnetic Resonance, vol. 45-46, pp. 36-44, (2012).

[2] D. Possa, A. C. Gaudio, and J. C. C. Freitas, "Numerical simulation of NQR/NMR: Applications in quantum computing," Journal of Magnetic Resonance, vol. 209, pp. 250-260, (2011).

1. Introduction

Nuclear magnetic and quadrupole resonance (NMR/NQR) have a long-standing reputation as accurate methods for the microscopic investigation of materials based on remarkably simple working principles. In addition to being a dominant tool in chemistry, materials science, structural biology, and medicine, NMR represents an essential tool in quantum information science (QIS) [1–3]. NMR can also be utilized for fundamental tests of quantum mechanics [4] and condensed matter physics, as well as for probing microscopic spin and charge properties of materials [5–8]. These features are the reason for the success of magnetic resonance techniques in implementing one of the first quantum information processors: the high degree of control of nuclear spins that they provide naturally leads to basic quantum computing, and has made it possible to witness the experimental realization of several quantum algorithms for the first time [9–17]. The handling of quantum systems to perform data processing tasks in NMR is accomplished through the application of specific radio frequency (RF) pulses (logic gates) on adequately prepared ensemble states, referred to as pseudopure states (PPS) [15,16,18–20]. The logic gates can be executed with high fidelity due to the superior level of control of the quantum evolution of nuclear spins. Indeed, a 12-qubit NMR based quantum computer holds a record for a large quantum computer, *i.e.* a high fidelity implementation of a quantum algorithm with coherent manipulation of 12 qubits [21]. Nonetheless, the long term interest in the applications of NMR in quantum computing has faded since NMR presents some major limitations when it comes to implementing a large scale quantum computer.

Unfortunately, NMR has not seen as much development in the strongly correlated materials community compared to other spectroscopic techniques in recent decades. The only place where NMR methodologies have kept on pace with our understanding of spin dynamics is as a control paradigm for quantum information technology (*e.g.* diamond-NV centers [22]). Much of that progress has been in the realm of quantum control and sensing, *i.e.* the creation of specially engineered pulse sequences that best extract information out of single-spin systems [23–27]. However, these protocols developed for the manipulation of NMR qubits (single-spin systems) promise to be valuable resources for the exploration of complex emergent properties of materials [28,29].

Here, we introduce unified protocols, presented in an open source software with a user-friendly interface, to enable the simulation of both standard NMR spectroscopic observables and the time-evolution of an interacting single-spin system subject to complex pulse sequences, *i.e.* quantum gates. Our software can simulate the acquisition of the characteristic observable measured in a laboratory for single-spin systems under different pulse sequences, such as the free induction decay signal (FID), and then generate the NMR/NQR spectrum in a form which can be directly compared to real experimental results. The program is adaptable to the simulation of a wide range of experimental outcomes, as it makes use of three different evolution solvers: *(i)* the time-independent Hamiltonian diagonal solver, *(ii)* the average Hamiltonian theory, implemented up to third order but easily extendable to higher orders as required, and *(iii)* QuTiP with its different master equations [30,31]. In addition, the program incorporates a quantum computing module that allows for the design of quantum circuit elements, relevant for both researchers and developers that focus on the direct, real-time interface with instrumentation for quantum control, such as the Quantum Orchestration Platform provided by Quantum Machines [32].

The goal of the program is to aid the development of novel NMR-based protocols for identification of emergent quantum orders, which can be elusive to standard experimental probes. Theoretically-identified, complex quantum phases of matter [33,34] may encode details of their intricate structure in NMR responses [35,36] in ways that lay outside the current NMR spectroscopy paradigm. Therefore, our computational tool is instrumental in designing the experiments (*i.e.* NMR pulse sequences) that optimize the sensitivity of an NMR observable to the intricate structure of correlated quantum states, as discussed in Sec. 4.5. Moreover, the extension of this work to ensembles of nuclei will be vital for providing relevant data to enable the reverse engineering of Hamiltonians of such quantum phases in strongly interacting materials [37,38]. Finally, this program can be beneficial when designing optimal control protocols for quantum sensing applications.

Realizing NMR protocols, which ultimately enable identifying quantum phases in complex materials via careful manipulation of nuclear spin degrees of freedom requires the development of software to simulate experimental techniques featuring the representation of nuclear spin states. Although there are many other NMR simulation programs, to our knowledge, most modern NMR/NQR software is mainly geared towards applications in chemistry, or is an add-on library to closed-source software. Some well liked, but aging programs that simulate NMR/NQR experiments are coded with less widely-used programming languages, such as SIMULDENS that uses VAS PASCAL [39], SIMPSON in the Tcl scripting language, while its core in the C programming language [40], WSOLIDS1 in Microsoft Visual C++ 2008 Express Edition [41], and WINDNMR-Pro, which is a stand-alone Windows programs whose development has ceased and whose source code is not publicly available [42]. A similar package to ours is the NMR/NQR simulation that includes elliptically polarized RF fields with preparation of pseudo-pure states and basic quantum gates, proposed by Possa et al. [43], but its source is inaccessible, and it requires the paid Wolfram Mathematica environment. Additional extensively used packages include SpinDynamica [44], also for Mathematica, and Spinach for MATLAB [45]. There exists other licensed software, such as SpinEvolution [46] and the PERCH software, a wholly-owned subsidiary of Bruker BioSpin [47]. Further, programs such as QUEST [48] and SPINUS [49] lack the density matrix visualization

of spin states. For completeness, we note that numerous software packages have been developed in the computational chemistry community, but these are mainly dedicated to molecular and protein structure determinations [50,51]. Therefore, our aim was to develop an up-to-date, open-source, extensively-documented software, written in the more popular programming language Python that combines and makes fully accessible all features relevant to physics research. Furthermore, our software is integrated with the fairly well known, highly efficient open-quantum-systems dynamics simulator, QuTiP [30,31], empowering it with even more capabilities. The reason for an initial independent framework is to better understand and account for the technical difficulties, as opposed to using an existing framework as a black box.

Our software PULSEE (Program for the simULation of nuclear Spin Ensemble Evolution) [52] is based on the quantum mechanical description of magnetic resonance and can simulate the time evolution of nuclear spins in a wide variety of configurations encountered experimentally. One way we calculate the dynamics of the spin system is in the interaction frame where the quantum states only evolve as a result of time-dependent pulses, which makes the program highly versatile in its application. Although this package was designed to handle non-interacting, single-spin systems in solids dominated by the Zeeman and quadrupolar interactions, the software can handle relevant coupling with other nuclei and/or electrons, simulating the evolution of single-spin systems subject to different pulse sequences. As such, the software is not intended to directly reproduce experiments that study correlations and/or entanglement in quantum materials, but rather to quantify the deviation of these experiments from an idealized single-spin evolution. Once established, one may proceed to determine the source of the novel phenomena. To directly investigate strongly correlated phases of matter, one may use other techniques and simulations of many-interacting spins. One such approach is a novel methodology in NMR that can probe the electronic susceptibility via the variation of the pulse strength and applied field orientation, which has direct applications in sensing and characterizing emergent electronic phases [36,53].

The paper is organized as follows: **Section** 2 gives an overview of the theory of NMR and NQR, including both the description of nuclear spin dynamics and the generation of the spectra from the analysis of the FID. **Section** 3 presents the simulation software, providing practical information about its installation, structure, and usage. **Section** 4 provides several examples of simulations carried out with PULSEE, which have been chosen for their relevance to quantum control and quantum information processing. Specifically, in **Section** 4.5 we illustrate how ideas developed in the context of QIS can be deployed to efficiently probe the complexity of the hyperfine tensor arising as a result of intricate interactions in the emergent quantum phases of matter [33,34,54,55].

2. Theoretical background

Nuclear magnetic and quadrupole resonance (NMR/NQR) involve the time evolution of resonantly perturbed nuclear spins. Experimentally, the distinction between the two methods lies in the different nuclear interactions being probed: NMR pertains to nuclei coupled to a local magnetic field (that is, an externally applied magnetic field), while NQR deals with the quadrupolar interaction between each nucleus and the surrounding electronic charges. From a theoretical point of view, it is convenient to treat the problem where both interactions are simultaneously present, since it includes all the possible intermediate configurations between pure NMR and pure NQR. In addition, the system may include other less significant interactions that influence its evolution, such as dipole-dipole and hyperfine interactions, chemical and paramagnetic shifts, J-coupling, and gradient fields [7].

Although we aim to understand correlated systems, it is more beneficial to study single-spin, non-interacting systems, and gradually include interactions. The stationary Hamiltonian at thermal equilibrium is given by:

$$\mathcal{H}_{full} = \mathcal{H}_Z + \mathcal{H}_Q + \mathcal{H}_{HF} + \mathcal{H}_{CS} + \mathcal{H}_D + \mathcal{H}_J + \mathcal{H}_{other}. \tag{1}$$

Here, $\mathcal{H}_Z$ and $\mathcal{H}_Q$ stand for the dominant Zeeman and quadrupolar interaction terms, respectively. The next four terms, $\mathcal{H}_{HF}$, $\mathcal{H}_{CS}$, $\mathcal{H}_D$, and $\mathcal{H}_J$, are the hyperfine interaction, chemical shift, dipole-dipole interaction, and J-coupling, respectively, and their relevance is material-specific. The last term $\mathcal{H}_{other}$ includes any other potential time-independent interactions. The Zeeman term represents the direct coupling between the nuclear intrinsic magnetic moment $\gamma\hbar\mathbf{I}$ and the externally applied magnetic field $\mathbf{B}_0$:

$$\mathcal{H}_Z = -\gamma\hbar\mathbf{I}\cdot\mathbf{B}_0, \tag{2}$$

where γ is the gyromagnetic ratio of the spin and $\hbar\mathbf{I}$ is the spin operator of the nucleus. The term $\mathcal{H}_Q$ represents the interaction between the electric quadrupole moment of the nucleus and the electric field gradient (EFG), generated by the surrounding electrons, represented by a 3x3 tensor $\mathbf{V}(\Theta)$, is given by

$$H_Q = \frac{eQ}{2I(2I-1)}\mathbf{I}\cdot\mathbf{V}(\Theta)\cdot\mathbf{I}. \tag{3}$$

In the coordinate system of the principal axis of the EFG it reads:

$$\mathcal{H}_Q = \frac{e^2qQ}{4I(2I-1)}\left(3I_Z^2 - I(I+1) + \frac{1}{2}\eta(I_+^2 + I_-^2)\right), \tag{4}$$

where I is the nuclear spin number, e is the elementary charge, $eq = V_{ZZ}$ is the largest eigenvalue of the EFG tensor, eQ is the electric quadrupole moment, and η is the asymmetry parameter of the EFG. In strongly correlated materials, the next most important term is the hyperfine coupling, which describes the interaction of the nuclear spin with that of the electron and includes a dipole-dipole interaction and Fermi contact term, given by

$$\mathcal{H}_{HF} = \mathbf{S}\tilde{A}\mathbf{I}, \tag{5}$$

where $\mathbf{S}, \mathbf{I}$ are the electronic/nuclear spin operators, respectively, and $\tilde{A}$ is the hyperfine tensor [7]. The other interaction terms and their secular approximations are described in Appendix A.

In NMR/NQR, one probes these interactions by sending a pulse of radiation onto the system, which accounts for a perturbing term to be included in the full Hamiltonian:

$$\mathcal{H}_1(t) = (2\mathbf{B}_1\cos(2\pi\nu_P t - \varphi_P))\cdot\mathbf{I} \tag{6}$$

where $2\mathbf{B}_1$ is the magnetic component of the radiation pulse, ν_P and φ_P are the pulse's frequency and phase, respectively. This B_1 radiation field is in a plane perpendicular to the externally applied static magnetic field, B_0, that defines the Zeeman quantization axis.

Before the application of any pulses, the system is in a thermal equilibrium state, $\rho(t_0 = 0)$, which at room temperature is approximated as

$$\rho(0) = \exp(-\mathcal{H}_0/k_BT)/\mathcal{Z} \approx (1 - \mathcal{H}_0/k_BT)/\mathcal{Z} \tag{7}$$

The software uses numerical methods to calculate the exponential of a matrix up to a high precision, instead of just using the first-order term of the Taylor expansion. Computing the evolution of this state under the action of a pulse is equivalent to finding the corresponding evolution operator $U(t_P, 0)$, where t_P is the time duration of the pulse. In the most general case, this

operator cannot be computed directly, since the full Hamiltonian $\mathcal{H} = \mathcal{H}_0 + \mathcal{H}_1(t)$ may depend on time. Here, $\mathcal{H}_0$ encompasses only the terms of the full Hamiltonian specific to the problem to be simulated.

2.1. Computing the spin dynamics

The program has three main modes to evaluate the system dynamics, that is, evaluating the effects of the time evolution operator:

i **Direct diagonalization** of the unitary evolution operator.
The method is intended for low-dimensional spin Hilbert spaces and time-independent Hamiltonians, where pulses are modeled as instantaneous rotation operators.

ii **Average Hamiltonian Theory (AHT)** up to 3rd order in the Magnus expansion.
The AHT approach is appropriate for time-dependent Hamiltonians whenever the Zeeman interaction is dominant, ensuring that the Magnus expansion converges. Evidently, this method fails for modeling Zeeman perturbed NQR.

iii Using **QuTiP**'s solvers which support collapse operators and non-unitary evolution for efficient simulation of dynamics of open quantum systems.
This is the most general and resource-demanding method that can handle extensive range of time-dependent Hamiltonians. One can improve the QuTiP backend's efficiency by compiling with the optional Cython and parallelization dependencies.

The user can readily choose the optimal mode for their intended implementation and appropriate evaluation of the spin dynamics. We point out that a full simulation of any realistic material is impossible because of the huge dimension of the resulting Hilbert space ($(2I+1)^N$, where N is the number of interacting spin-I nuclei). Instead, spin dynamics are modeled by effective spin components that can be calculated in a highly reduced Hilbert space of just a handful of spins.

i. Direct Diagonalization

Even though this high-precision, high-performance solver is designed for time-independent Hamiltonians, it supports modeling NMR pulses as instantaneous operators that represent a spin rotation. The advantage of this approach is that the precision is independent of the time steps used. The floating point precision is the only limiting factor: the dynamics of the system are governed by the time evolution operator, $U(t)$, for the initial state, $|\psi(0)\rangle$, of the following form,

$$\psi(t) = U(t)\psi(0) = e^{-i\mathcal{H}t/\hbar}\,|\psi(0)\rangle\,, \tag{8}$$

while in the density matrix formalism, one utilizes the von Neumann equation for the initial density matrix, $\rho(0)$, to obtain

$$\rho(t) = e^{-i\mathcal{H}t/\hbar}\rho(0)e^{i\mathcal{H}t/\hbar}. \tag{9}$$

Such dynamics can then be simulated by executing the matrix diagonalization directly. This method is a powerful and efficient tool for a fairly good approximation of NMR dynamics.

The RF pulses are considered idealized spin rotation operators in the direct diagonalization method. Thus, a pulse of angle α, applied along some direction, $\hat{I}$, is represented by

$$\mathcal{R}(\alpha) = \exp\{-i\alpha\hat{I}\}, \tag{10}$$

where $\hat{I}$ is the axis along which the spins are rotated. We note that one could model the time-dependent RF pulses within the exact diagonalization approach by dividing the Hamiltonian into small time-steps in which each Hamiltonian is treated as time-independent. However, if the time-discretization is too fine, the exact diagonalization approach will no longer have a performance improvement over average Hamiltonian theory. Therefore, we recommend that the Magnus expansion be used to investigate the effect of finite pulses.

An example of a functional application of the direct diagonalization mode is the implementation of quantum computing protocols for electron-nuclear systems, readily attainable by using the hyperfine coupling (Eq. (5)) [56]. Successful coherent control of such electron-nuclear systems achieved through a highly-detailed simulation of the system's dynamics can facilitate the realization of robust quantum gates. Such a simulation, in some measure, is difficult because of the three orders of magnitude difference between nuclear and electronic spin gyromagnetic ratios. Using numerical methods to simulate the dynamics would require the use of a time-step size congruent with the particular timescale of the system, set by for example, the dominant Zeeman interaction for systems placed in a strong magnetic field. The Zeeman interaction of electron-nuclear system is represented by,

$$\mathcal{H}_0 = -\omega_n(I_z \otimes \mathbb{1}) - \omega_s(\mathbb{1} \otimes S_z), \tag{11}$$

where ω_n, ω_s are the nuclear and electronic Larmor frequencies, respectively. The standard NMR procedure would be to solve the dynamics of the system in the rotating frame of the nucleus. However, since the electronic Larmor frequency is three orders of magnitude greater than the nuclear one, passing to the rotating frame of the nucleus is to no avail. Employing the direct diagonalization mode, one can surpass these issues because the dynamics of the system can be evaluated at each step, independent of each other. Any digitization issues can be easily overcome by including more points in the time array. The parallelization in Python can be used to enhance the program's performance if speed-up is necessary.

Even so, the direct diagonalization method can become time-consuming as the dimensions of the relevant Hilbert space increase. This problem can be somewhat overcome by the parallelization process in Python, and by using sparse matrices. Nevertheless, direct diagonalization is practically impossible for systems with large Hilbert spaces, and additionally modeling dissipation would be a daunting task. For such endeavors, we turn to alternative numerical methods.

ii. Average Hamiltonian Theory

In most NMR applications, the dominant term is the Zeeman interaction, $\mathcal{H}_0 = \mathcal{H}_Z$, defining the so called *rotating frame* [57,58]. The procedure that this mode follows consists of two steps:

1. The problem is cast to the interaction frame, where the only relevant term of the Hamiltonian is the perturbing one:

$$\mathcal{H}(t) \to \mathcal{H}_{\mathcal{H}_0}(t) = \exp(i\mathcal{H}_0 t/\hbar)\mathcal{H}_1(t)\exp(-i\mathcal{H}_0 t/\hbar). \tag{12}$$

2. The evolution operator is approximated by retaining the number of terms of the Magnus expansion depending on the application [57,58], the first few of which are computed through the following formulas:

$$\Omega_1(t_P, 0) = \int_0^{t_P} dt_1 \widetilde{\mathcal{H}}(t_1) \tag{13}$$

$$\Omega_2(t_P, 0) = \frac{1}{2}\int_0^{t_P} dt_1 \int_0^{t_1} dt_2 [\widetilde{\mathcal{H}}(t_1), \widetilde{\mathcal{H}}(t_2)] \tag{14}$$

$$\Omega_3(t_P,0)=\frac{1}{6}\int_0^{t_P}dt_1\int_0^{t_1}dt_2\int_0^{t_2}dt_3\Big([\widetilde{\mathcal{H}}(t_1),[\widetilde{\mathcal{H}}(t_2),\widetilde{\mathcal{H}}(t_3)]]+ [\widetilde{\mathcal{H}}(t_3),[\widetilde{\mathcal{H}}(t_2),\widetilde{\mathcal{H}}(t_1)]]\Big) \quad (15)$$

where $\widetilde{\mathcal{H}}\equiv -i\mathcal{H}(t)/\hbar$, from which the evolution operator is readily computed up to n^{th} order, as

$$U(t_P,0)=\exp\Big(\Omega_1(t_P,0)+\Omega_2(t_P,0)+\Omega_3(t_P,0))+\cdots + \Omega_n(t_P,0)\Big). \quad (16)$$

The Magnus expansion has been implemented up to the 3rd order in the program as it was deemed adequate for a fast converging Hamiltonian, but this can be easily expanded up to the n$^{\text{th}}$ order.

iii. Subroutined QuTiP Solvers

To simulate open quantum systems (*i.e.* nuclear spins in a material), we have incorporated QuTiP Quantum Toolkit in Python [30,31] subroutines into the PULSEE solver modules. Developed as an open-source, efficient, and highly-optimized numerical simulator, this package includes different evolution equations, such as the Schrödinger's equation, Lindblad Master equation, Bloch-Redfield master equation, and a Stochastic Solver. The user can choose which one they deem most appropriate for the NMR simulation at hand, bearing in mind that some of these solvers are resource-intensive. The default solver invoked in PULSEE is the Lindblad master equation. Next, to facilitate correct employment of the subroutines, we review the important assumptions that give the form of the equation used by QuTiP. That is, we outline assumptions about the physical system that have to be satisfied in order for QuTiP's Lindblad master equation solver routine to be applicable.

The Lindblad master equation is a phenomenological and macroscopic formalism to describe the evolution of an open system interacting with its environment through "collapse operators," defined by operators that couple the system to a Markovian reservoir with corresponding rates [30,31]. The equation is trace-preserving and completely positive. If collapse operators are absent, it simply reduces to the Schrödinger's equation. As a general form of a Markovian master equations, the Lindblad master equation is applicable under the following assumptions:

1. **Separability.** Initially, the system and the environment are completely *uncoupled*, and the total density matrix is a tensor product of two parts $\rho_{\text{tot}}(0)=\rho(0)\otimes\rho_{\text{env}}(0)$.
2. **Born approximation - the weak coupling limit.** The environment is unaffected by the system, and the total density matrix can be written as a tensor product, $\rho_{\text{tot}}(t)\approx\rho(t)\otimes\rho_{\text{env}}$.
3. **Markovian reservoir.** Any excitations in the environment induced by the system, must decay quickly compared to the dynamics of the system itself.
4. **Secular & rotating wave approximation.** Fast oscillating terms in the master equation are neglected. In addition, any terms leading to a renormalization of the system's energy levels are ignored. Note that this last approximation is not necessary for all master equations, such as the Block-Redfield master equation [59,60].

Thus, it is essential that the system modeled using the Lindblad master equation is weakly coupled to the environment and it does not have degenerate energy levels. In addition, although using the sparse matrix formalism saves memory, the computation time of the master equation grows exponentially with the number of states [30]. Whenever the number of states exceeds 1000, it might be more appropriate to use QuTiP's Monte Carlo solver that has more efficient scaling properties [30,31].

In typical NMR/NQR simulations, the Lindblad master equation should be more than sufficient to effectively capture experimental results. For a more advanced use, such as microscopic modeling of dissipation and dephasing processes in spin systems, the user should switch to the Bloch-Redfield formalism. In this case however, the evolved density matrix might not be physical due to the perturbative nature of the method [59,61].

In short, using QuTiP circumvents the limitation of the time-independent direct diagonalization method. It also improves on the Magnus expansion, which converges poorly in some interaction regimes. What is more, QuTiP allows PULSEE to take advantage of both phenomenological (the Lindblad Master equation) and microscopic (the Bloch-Redfield equation) to model dissipation and properly account for dephasing, instead of an empirical decay function, such as the loss of magnetization via a function $\mathcal{M}(t,T_2)$, described below.

2.2. Simulating NMR observables

The PULSEE package can be used to generate and analyze typical observables measured in magnetic resonance experiments, such as the free induction decay signal (FID). In laboratories, the FID is the electrical signal induced in a coil wound around the sample after the electromagnetic RF pulse is switched off. This signal is proportional to the component of the sample's magnetization along the axis of the coil [62]. If the coil is oriented along $\hat{\mathbf{n}}$, then the FID signal will be given by:

$$S(t)=\text{Tr}\big[\rho(t)\ \hat{\mathbf{n}}\cdot\mathbf{I}\ \mathcal{M}(t,T_2)\big] \qquad t>t_P \quad (17)$$

where we replaced the magnetization with the spin operator $\mathbf{I}$ of a single nucleus in the ensemble, since they are equal up to a scaling factor, and we introduced an empirical functional form of the loss of magnetization, or the decay of signal, $\mathcal{M}(t,T_2)$, usually set to $\exp(-t/T_2)$. One can directly specify the form of the function, for example, a stretched exponential, or pass in as many parameters (decoherence times (T_2), stretching exponents β, etc) as necessary to mimic desired decays. In effect, our software generates a complex FID whose imaginary part represents the signal induced in an "additional" coil in-plane orthogonal to $\hat{\mathbf{n}}$. The general complex FID reads $S(t)=\text{Tr}[\rho(t)\ \ I_+\ \ \mathcal{M}(t,T_2)]$.

One then typically computes its Fourier transform to obtain an NMR/NQR spectrum. This is the main outcome of the experiment and provides information about the interactions experienced by the system and the energy transitions that occurred in its evolution. This is shown by the expansion of the FID in its Fourier components:

$$S(t)=\sum_{\varepsilon,\eta}\langle\varepsilon|I_+|\eta\rangle\ \langle\eta|\rho(t_P)|\varepsilon\rangle\exp\big(i\omega_{\varepsilon,\eta}t\big) \quad (18)$$

where ε, η run over the energy eigenvalues of the system, $|\varepsilon\rangle$, $|\eta\rangle$ are the corresponding eigenstates, and $\omega_{\varepsilon,\eta}$ is the frequency of transition between these two. This formula shows that the peaks of the NMR/NQR spectrum are located at the resonance frequencies $\omega_{\varepsilon,\eta}$, and that some of these frequencies may not show up in the spectrum if the associated transition has not occurred, or if the detection setup (*i.e.* coil) is not oriented properly. In addition, comparison with the experimental spectrum may reveal the deviation of the actual system from the ideal theoretical case, generating a basis for further study.

3. Structure and usage of the software

PULSEE is not simply a simulator of the time evolution of nuclear spin states, but also reproduces all the main observable features of NMR/NQR experiments. In this way, the program is a valuable tool in experimental research because the outcomes of a simulation are generated in a form that can be directly compared with the results measured in a laboratory.

Numerical simulations are prone to errors due to assumptions in approximations and in numerical absolute tolerance if pushed beyond their intended use. In order to ensure full control over PULSEE and a reliable reproduction of results, we have opted for a completely independent implementation, in addition to an integration with an already-exiting framework, such as QuTiP [30,31], to fully grasp any potential numerical artifacts. In particular, we noticed that the 2nd order Magnus expansion was insufficient in the interaction (Dirac) frame, but sufficient in the rotating reference frame (RRF), induced by $\mathcal{O}_{RRF} = \hbar\omega I_z$. By going to a higher order in the Magnus expansion, the two pictures converged, demonstrating the necessity of being able to access and change the source-code of the program. Moreover, there is a great benefit to incorporating PULSEE and QuTiP because of the relevant extra features already developed.

Another source of error in NMR simulation software is the discrepancy between simulated and measured results arising from deviations from idealized/instantaneous pulses and the absence of noise normally encountered in experiments. PULSEE allows both the effect of finite pulse and the noise on observables to be investigated. Specifically, we address the effects of the pulse duration by evolving the system under the influence of the relevant Hamiltonian for the appropriate time that corresponds to that of the desired pulse. Such an evolution introduces noise, especially when handling more complicated interactions. Because instantaneous pulses are pertinent for the QIS community, we have developed a module that allows for the simulation of idealized quantum circuits and gates (Sect. 4.6). Furthermore, PULSEE can be deployed to simulate field inhomogeneities, as well as distributions in different parameters, such as the quadrupolar coupling term, and the Zeeman term, by averaging over multiple Hamiltonians, effectively simulating environmental noise. This is another functional feature which was included to assist in the design of optimal noise spectroscopy protocols [63–67].

3.1. Download, dependencies and launching

The software can be downloaded from the following GitHub repository: https://github.com/vemiBGH/PULSEE

PULSEE has been written entirely in Python 3.7. One must install PULSEE by navigating to the directory where the file setup.py is located, and by running

```
$ pip install -e.
```

The program makes wide use of many of the standard Python modules (namely `numpy`, `scipy`, `pandas`, `matplotlib`) for its general purposes, as well as the Quantum toolkit in Python (`QuTiP`) [30]. We strongly recommend using the Anaconda distribution. Tests have been carried out using the `pytest` framework and the `hypothesis` module. The software includes a GUI which has been implemented with the tools provided by the Python library `kivy`. In addition, it is highly recommended that QuTiP's `parallel computation` module is used as it dramatically reduces the runtime, especially for the direct diagonalization method, by spawning processes and fully leveraging multiple processors on a given machine.

The two different GUIs are launched from the directory `src/pulsee` by entering the following command in the terminal

```
$ python PULSEE_CMP_GUI.py
$ python PULSEE_CHEM_GUI.py
```

The use of the GUI is strongly discouraged and only suggested as a 'quick-and-dirty' modeling technique. Otherwise, one is strongly advised to use the functions defined in the module `Simulation` to write a custom simulation, as outlined in subsection 3.3. To give more freedom to the user and appeal to a wider audience more familiar with Mathematica, we have written Jupyter notebook demos that are easy to adapt to the system under investigation.

3.2. Modules of the software

The program consists of 6 modules. The content and role of each module is briefly described, below:

1. `Operators`
   This module, together with `Many_Body`, can be considered as a toolkit for the simulation of generic quantum systems. It contains the definition of Python classes and functions related to the basic mathematical objects which enter in the treatment of a quantum system. `Operators` simulates a single spin system, while `Many_Body` extends to multiple spins.
2. `Many_Body`
   Among other things, `tensor_product` and `partial_trace` transform a single particle Hilbert space to a many-particle space, and vice-versa.
3. `Nuclear_Spin`
   Defines classes representing the spin of an atomic nucleus or a system of nuclei.
4. `Hamiltonians`
   Defines relevant terms of the Hamiltonian of a nuclear spin system in a typical NMR/NQR experiments: the Zeeman and quadrupolar interactions, full J-coupling between nuclei using the J tensor or J-coupling in the secular approximation, isotropic chemical shift in the secular approximation, dipolar for homonuclear and heteronuclear spin-spin interactions, hyperfine interaction in the secular approximation, any interaction that can be represented with a tensor between two spins, and interaction with an RF radiation pulse. Finally, the program allows the input of a square matrix as a `numpy` array that represents any predefined Hamiltonian.
5. `Simulation`
   This is the module the user should refer to in order to implement a custom simulation. The functions defined here allow the user to set up the nuclear system, evolve it under a sequence of pulses, generate the time domain response/signal, and compute the NMR spectrum.
6. `Quantum_computing`
   Implements fundamental components of quantum circuits, including several quantum gates, and `Qubit` objects, acted upon by gates. In principle, the user may construct and manipulate elementary quantum circuits, and extract relevant information, such the final density matrix of the composite qubit state.
7. `NMR_NQR_GUI`
   There are two versions of the graphical user interface (GUI) depending on the application. The condensed matter physics (CMP) `PULSEE_CMP_GUI` deals only with a single-spin system that is governed by the Zeeman & Quadrupolar interactions. The second `PULSEE_CHEM_GUI` extends the single-spin system to include weaker couplings in the secular approximations by considering a generalized secondary spin. Although the GUI provides a simple and intuitive way to perform a simulation, it has limited features regarding a custom simulation

code that can reproduce complicated experiments involving complex multi-pulse sequences.

3.3. Building up a simulation

The starting point of any simulation is the set up of the system under study, which is done by calling the function `nuclear_system_setup`:

```
nuclear_system_setup(spin_par, quad_par=None,
 zeem_par=None, \
 j_matrix=None, cs_param=None, D1_param=None, \
 D2_param=None, hf_param=None,
 h_tensor_inter=None, \
 j_sec_param=None, h_userDef=None, \
 initial_state='canonical', temperature=1e-4)
```

This function returns three objects representing the spin system, the unperturbed Hamiltonian, and the initial state, respectively.

The next step is to evolve the state of the system under the action of a radiation pulse, a task carried out by the function `evolve`:

```
evolve(spin, h_unperturbed, dm_initial,
       solver=mesolve, \
       mode=None, pulse_time=0, \
       picture='RRF', RRF_par={'nu_RRF': 0,
                               'theta_RRF': 0,
                               'phi_RRF': 0},\
       n_points=30, order=None, opts=None,):
```

The function allows the user to specify not only the features of the pulse applied to the system, but also the reference frame in which the evolution is computed for the AHT solver.

Once the evolved state is obtained from `evolve`, one can generate the FID signal associated with this state by calling the function `FID_signal`:

```
FID_signal(spin, h_unperturbed, dm,
           acquisition_time, T2=100, \
           theta=0, phi=0,
           reference_frequency=0, n_points=30)
```

The arguments of this function allow the user to set the time window of acquisition of the FID, the decoherence time T_2, and the frequency and orientation of the detection coils.

Eventually, one computes the NMR/NQR spectrum from the FID signal by passing the FID through the function `fourier_transform_signal`:

```
fourier_transform_signal(signal, times,
                         abs=False, padding=None)
```

The module `Simulation` also includes the functions for plotting the density matrix of the evolved state as well as the FID signal and NMR/NQR spectrum.

4. Examples of execution

In this section we illustrate some noteworthy simulations performed with PULSEE. In addition to being valid examples of the execution of the code, these simulations have been chosen because they clearly demonstrate the precision of NMR and NQR in the control of nuclear spin degrees of freedom, which reflects their accuracy in the determination of unknown nuclear interactions in a sample under study.

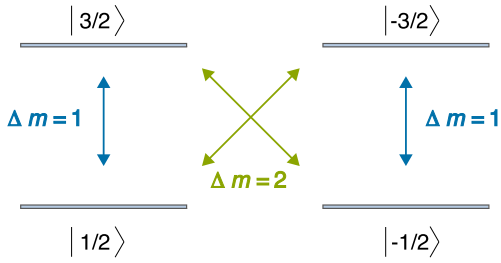

Fig. 1. Schematic of the energy spectrum and the possible transitions of a nuclear spin 3/2. The transitions labeled with $|\Delta m| = 1$ involve the exchange of a single photon, while those labeled $|\Delta m| = 2$ denote a two photon process.

4.1. Selective transitions between quadrupolar states by means of properly polarized pulses in NQR experiments

The structure of the energy spectrum of quadrupolar nuclei allows for the selective excitation of its states by applying a pulse of radiation with the proper polarization.

A first notable example is represented by the pure NQR of a spin 3/2 nuclei whose energy levels and available transitions are depicted in Fig. 1. This system may undergo two single photon transitions at the same frequency, namely $|1/2\rangle \leftrightarrow |3/2\rangle$ and $|-1/2\rangle \leftrightarrow |-3/2\rangle$. This is in contrast with a pure NMR experiment where all the transitions are characterized by the same variation of the magnetic quantum number Δm. These two transitions imply an opposite change in the angular momentum of the system, so that each of them can occur only under the exchange of a photon with circular polarization (c.p.) σ^+ and σ^-, respectively. Therefore, when one irradiates the system by a linearly polarized (l.p.) resonant pulse, both transitions will be induced. In contrast, by choosing the proper polarization of the pulse one is able to select only one of the two. The potential of circularly and, in general, elliptically polarized RF pulses in NQR has been widely explored [68–70].

These theoretical expectations are correctly reproduced by our software. We simulated the pure NQR of a spin 3/2 ^{35}Cl nuclei in a potassium chlorate crystal ($KClO_3$), whose gyromagnetic ratio is $\gamma/2\pi = 4.17$ MHz/T and whose quadrupolar resonance frequency is $\nu_Q = 28.1$ MHz [71]. We prepared the system in the initial state depicted in Fig. 2. Then, we performed two distinct simulations evolving the system under the action of a π pulse with polarization σ^+ or σ^- respectively (in a classical picture such pulses rotate the initial nuclear magnetization by 180°, clockwise and anticlockwise, respectively). The results obtained are shown in Fig. 3. We note that the π pulse is defined such that its amplitude, B_1, and time duration, t_P, satisfy the equation known as a central-transition selective pulse

$$\gamma \alpha B_1 t_P = \pi \tag{19}$$

where $\alpha = \sqrt{I(I+1) - m(m+1)}$ is a factor depending on the transition being induced, and thus differs between the central and satellite peaks, and γ is the gyromagnetic ratio of the nucleus. For the pulsing to be successful, the strength of the applied pulse γB_1 must be smaller than the quadrupolar frequency ω_Q. If the applied pulse is not perturbative relative to the quadrupolar energies, then the level mixing will occur instead of a simple spin rotation.

The evolved density matrices clearly show that a pulse with circular polarization σ^+ (σ^-) couples only with the transition between states $|1/2\rangle \leftrightarrow |3/2\rangle$ ($|-1/2\rangle \leftrightarrow |-3/2\rangle$) by acting selectively on the two relevant energy eigenstates to induce a full inversion of their respective populations and conserve the total angular momentum.

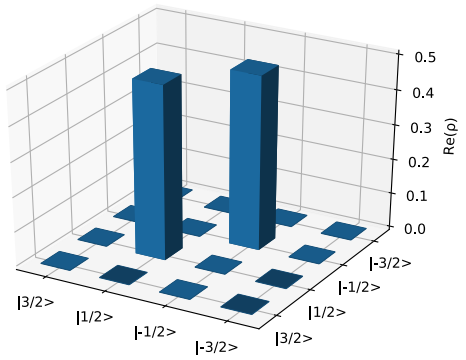

Fig. 2. Real part of the density matrix representing the initial state of the spin 3/2 nucleus in the simulation of a pure NQR experiment. The system is prepared in a classical distribution where the two ground states are equally populated.

Another experiment where a pulse can be designed to selectively induce transitions is the NQR of a spin-1 nucleus in the presence of an asymmetric EFG [7]. Due to the non-vanishing asymmetry parameter, the energy eigenstates of this system are no longer the spin eigenstates, but they read:

$$|0\rangle \qquad \& \qquad |\xi_\pm\rangle = (|1\rangle \pm |-1\rangle)/\sqrt{2} \tag{20}$$

The energies of these states and the frequencies of transitions between them are displayed in Fig. 4.

What is peculiar in this system is that in order for each of the three transitions to occur, the pulse must have a distinct linear polarization. Calculations show that

$$I_x = \begin{array}{c} \begin{matrix} |\xi_+\rangle & |0\rangle & |\xi_-\rangle \end{matrix} \\ \begin{pmatrix} 0 & 1 & 0 \\ 1 & 0 & 0 \\ 0 & 0 & 0 \end{pmatrix} \end{array} \begin{matrix} |\xi_+\rangle \\ |0\rangle \\ |\xi_-\rangle \end{matrix}$$

$$I_y = \begin{pmatrix} 0 & 0 & 0 \\ 0 & 0 & 1 \\ 0 & 1 & 0 \end{pmatrix} \quad I_z = \begin{pmatrix} 0 & 0 & 1 \\ 0 & 0 & 0 \\ 1 & 0 & 0 \end{pmatrix} \tag{21}$$

from which it is easy to prove that an $\hat{\mathbf{x}}$-, $\hat{\mathbf{y}}$- or $\hat{\mathbf{z}}$-polarized pulse will only affect the transition $|\xi_+\rangle \leftrightarrow |0\rangle$, $|\xi_-\rangle \leftrightarrow |0\rangle$, or $|\xi_+\rangle \leftrightarrow |\xi_-\rangle$, respectively. This behavior can be assessed by observing the spectrum generated by each of these pulses, recalling Eq. (18). Once the proper orientation of the detection coils is set, one is able to visualize if a certain transition has occurred depending on the whether the term $\langle\eta|\rho(t_P)|\varepsilon\rangle$ vanishes or not.

These results have been simulated in a fictitious spin 1 nucleus with $e^2qQ/h = 1\,\text{MHz}$ and asymmetry $\eta = 0.6$, for which the transition frequencies are $\nu_x \equiv \nu_{\xi_+\leftrightarrow 0} = 0.9\,\text{MHz}$, $\nu_y \equiv \nu_{\xi_-\leftrightarrow 0} = 0.6\,\text{MHz}$, and $\nu_z \equiv \nu_{\xi_+\leftrightarrow\xi_-} = 0.3\,\text{MHz}$. The resulting NQR spectra are displayed in Fig. 5.

4.2. Generation of quantum coherences in a spin 3/2 quadrupolar nucleus

Let us consider the ^{35}Cl nucleus with spin 3/2 in the same $KClO_3$ crystal introduced above. The previous example shows how to induce a full inversion of the populations of two of its energy eigenstates, say $|m = 1/2\rangle$ and $|m+1 = 3/2\rangle$, by means of a σ^+ c.p. π pulse of radiation. In general, when the angle on the right-hand side of Eq. (19) is set to a value different from $n\pi$, where n is an integer, the final density matrix exhibits non-zero off-diagonal elements, meaning that the evolved state includes a quantum superposition of $|m\rangle$ and $|m+1\rangle$. Such superposition states can be deployed to probe nature of tensor multipolar orders [33,55]. In NMR, such elements are typically called "single quantum coherences", where "single" specifies the fact that $\Delta m = 1$.

In Fig. 6, we display the results of three simulated experiments where a pulse resonant with the $|1/2\rangle \leftrightarrow |3/2\rangle$ transition is applied and the angle in Eq. (19) is set to the values $\pi/3$, $\pi/2$, and $2\pi/3$, respectively. These simulations demonstrate that it is possible to fine-tune the amplitudes of two states linked by a single-photon transition through the careful manipulation of the parameters of the pulse.

4.3. Preparation of an ensemble of spin 3/2 nuclei in a pseudopure state by means of NQR

NMR and NQR are naturally suited for the implementation of simple quantum information processors, as they are an efficient and high-precision method for manipulating nuclear spins [18,72–75]. Nonetheless, in typical NMR/NQR experiments the system under study is a macroscopic sample made up of a huge number of nuclei, which makes it impossible to prepare it in a pure state as would be required by an ordinary quantum computation protocol. This problem has been addressed by following a different strategy [9]: with a properly designed pulse sequence, the ensemble of nuclear spins can be prepared in a pseudopure state, *i.e.* a state $\rho = a\mathbb{1} + b\,|\psi\rangle\langle\psi|$ which differs from a pure state by a term proportional to the identity. A state of this kind is called pseudopure because, under evolution, it behaves like a full-fledged pure state. This property makes it the ideal starting point for any NMR/NQR quantum computation protocol. Indeed, much effort has been made in realizing quantum logic gates [2,15,76–84].

In what follows, we describe a simulation of the NQR protocol aimed at realizing a 2-qubit pseudopure state in the ensemble of ^{35}Cl spin 3/2 nuclei of a $KClO_3$ crystal [43], whose energy levels and available transitions have already been shown in Fig. 1. The states of the 2-qubit computational basis correspond to the spin ones as follows:

$$\begin{aligned} |00\rangle &\equiv |3/2\rangle \\ |01\rangle &\equiv |1/2\rangle \\ |10\rangle &\equiv |-1/2\rangle \\ |11\rangle &\equiv |-3/2\rangle\,. \end{aligned} \tag{22}$$

Here, we remark that the simulated protocol is not aimed at implementing the pseudopure state in the physical system itself. Such a state is obtained as the average of the results of three distinct experiments, as depicted in Fig. 7, following a common practice employed in NMR/NQR called temporal averaging [85]. In each of the three experiments, the system is handled in a distinct way:

1. In the first, the system is left in its original thermal equilibrium state.
2. In the second, the system is irradiated by a c.p. pulse with resonant frequency $\nu_Q = (E_{\pm 3/2} - E_{\pm 1/2})/h$, inducing one of the single photon transitions ($|\Delta m = 1|$). The time duration of the pulse is set to a value such that the populations of the states linked by the transition are exchanged.
3. In the third, a c.p. pulse at half the resonance frequency is applied, yielding one of the two-photons transitions ($|\Delta m = 2|$). Again, the time duration of the pulse accounts for the exchange of the populations of the states linked by the transition.

If the polarization of the pulses applied in steps 2 and 3 is appropriately chosen, the average of the density matrices resulting from the three experiments will have the properties of a pseudopure state belonging to the computational basis in Eq. (22). The outcome of the simulation, illustrating the real part of the density

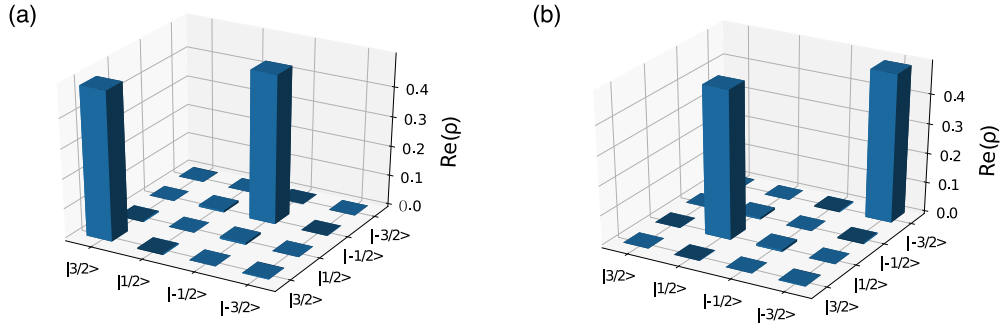

Fig. 3. Real part of the simulated density matrix representing the evolved state of the spin 3/2 quadrupolar nucleus after: (a) a π pulse with polarization σ^+; (b) a π pulse with polarization σ^-.

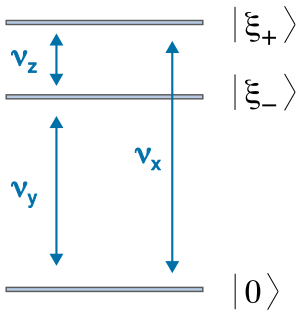

Fig. 4. Scheme of the energy spectrum and the available transitions for a quadrupolar nucleus of spin 1 interacting with an asymmetric EFG. The subscripts of the transition frequencies $\nu_{x/y/z}$ refer to the direction of linear polarization of the pulse required to induce each transition.

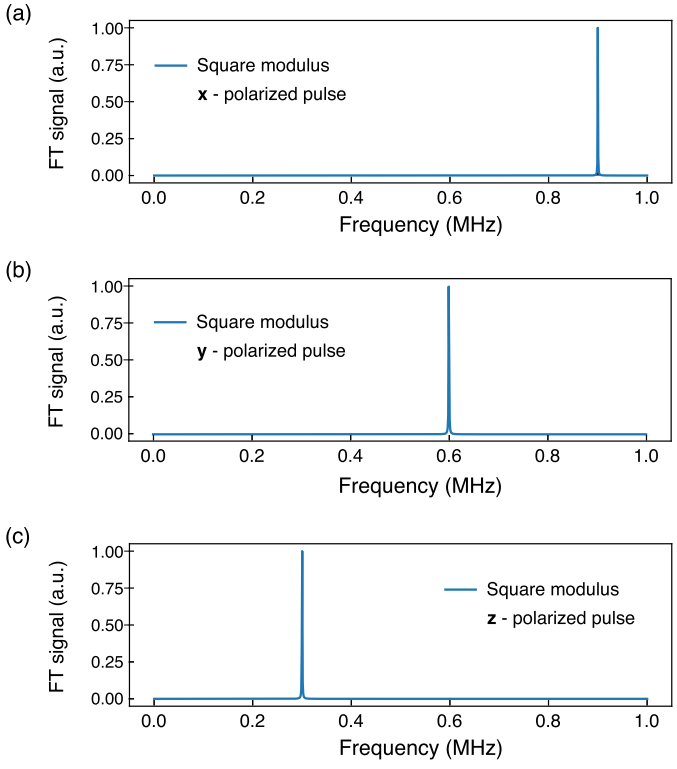

Fig. 5. Spectra resulting from three distinct simulations of the NQR of a spin 1 nucleus interacting with an asymmetric EFG, where different pulses have been applied with polarization along $\hat{\mathbf{x}}$ (a), $\hat{\mathbf{y}}$ (b), and $\hat{\mathbf{z}}$ (c), respectively.

matrices representing the four pseudopure states of the computational basis of 2 qubits, is shown in Fig. 8.

4.4. NQR and NMR implementation of a CNOT gate on a couple of qubits

Implementing a CNOT gate in the system we have already discussed in subsection 4.3 is a straightforward task. That is, in a 2-qubit system with $|0\rangle$ and $|1\rangle$ as the only allowed input values for both qubits, the CNOT gate flips the second (target) qubit from $|0\rangle$ to $|1\rangle$ if and only if the first (control) qubit is in the $|1\rangle$ initial state. Indeed, one can easily check that the action performed by a CNOT_1 gate on the 2-qubit system is equivalent to that of a pulse which yields an exchange of the populations between the states $|-1/2\rangle$ and $|-3/2\rangle$, as illustrated in Fig. 9a. The effect of this gate simulated by our software is depicted in Fig. 9b.

It is possible to implement an analogous operation by means of NMR as well, but in a different nuclear system. As explained in [18], this time the 2 qubits are encoded in 2 distinct spin 1/2 nuclei (following the convention $|0\rangle \equiv |1/2\rangle$, $|1\rangle \equiv |-1/2\rangle$) and, in order for them to work as a control-target qubit couple, they must interact with each other. Thus, we assume that they are linked by the typical J-coupling, whose contribution to the Hamiltonian is:

$$\mathcal{H}_J = hJ I_z^{(1)} I_z^{(2)} \tag{23}$$

where J is the coupling constant and $I_z^{(i)}$ is the z component of the spin of the i-th nucleus. The experimental protocol for the implementation of an NMR CNOT gate employs both selective rotations of each spin as well as the free evolution of the whole system under the action of J-coupling, according to the sequence:

$$\text{CNOT}_1 = \left(-\frac{\pi}{2}\right)_z^{\mathbf{I}_1} \left(\frac{\pi}{2}\right)_z^{\mathbf{I}_2} \left(-\frac{\pi}{2}\right)_x^{\mathbf{I}_2} U\left(\frac{1}{2J}\right) \left(-\frac{\pi}{2}\right)_y^{\mathbf{I}_2}. \tag{24}$$

Here, factors of the type $(\alpha)_{x/y/z}^{\mathbf{I}_i}$ represent pulses resonant with the i-th spin which make it rotate an angle α around the axis specified in the subscript. $U(1/2J)$, on the other hand, stands for the free evolution of the system for a time duration of $1/2J$. We point out that in order to be able to perform selective rotations of one of the two spins, the nuclei's gyromagnetic ratios must be appreciably different, leading to well separated gyromagnetic frequencies $\nu_0^{(i)} = -(\gamma^{(i)}/2\pi)B_0$.

We have carried out a simulation of this protocol starting from ideal pure input states. The outcomes match closely our expectations, *i.e.* the qubit is flipped since the control (first) qubit was in the $|1\rangle$ initial state, as is shown in Fig. 10.

4.5. NMR probe of quantum correlations and tensor orders

As a local probe, NMR is well suited for the study of the microscopic electronic spin structure in the vicinity of the nuclear spin

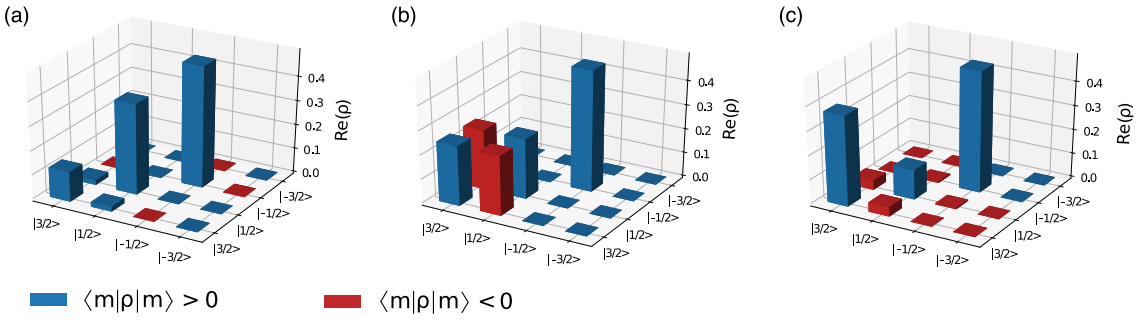

Fig. 6. Results of the simulation of the NQR of ^{35}Cl nuclei in a $KClO_3$ crystal where a pulse resonant with the $|1/2\rangle \leftrightarrow |3/2\rangle$ transition is applied. The three histograms show the real part of the density matrix of the system evolved after (a) $\pi/3$ pulse, (b) $\pi/2$ pulse, and (c) $2\pi/3$ pulse. As the angle of rotation approaches π, the populations of the states involved in the transition undergo a continuous exchange, and at the same time non-zero, off-diagonal elements emerge between them, meaning that the two states are in a quantum superposition.

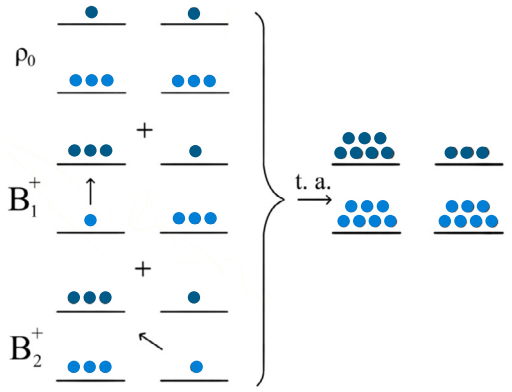

Fig. 7. Population diagrams of the states to be combined through temporal averaging in order to realize the $|11\rangle = |-3/2\rangle$ pseudopure state for a spin 3/2 quadrupolar nucleus.

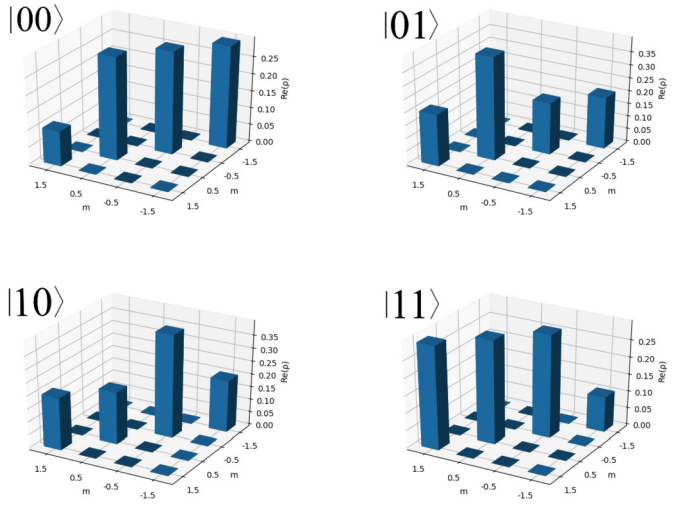

Fig. 8. Outcomes of the protocol for the realization of pseudopure states in an ensemble of spin 3/2 quadrupolar nuclei, as simulated by our software. The histograms display the real part of the density matrices representing the four pseudopure states of the computational basis of 2 qubits.

site through the hyperfine interaction. While directly measuring quantum correlations between electronic spins is difficult, complex hyperfine interactions can imprint signatures of electronic correlations on the nuclear spin states. The resulting many-body nuclear spin correlations can then be probed using the method of multiple quantum NMR [86–88]. The main challenge with this effort is that nuclear spin states are not pure states precluding the direct application of standard quantum protocols, which can be addressed by use of pseudo-pure states (sec. 4.3). PULSEE can be instrumental in designing the optimal multiple quantum NMR sequence to permit the study of quantum correlations.

Many of the theoretically identified complex quantum phases of materials are characterized by tensor orders (e.g. ferro-octupolar order) [33,34,89] that possess zero local susceptibility, and therefore, are evasive to standard experimental probes. However, the tensor nature of the hyperfine interactions can reveal the intricate structure of quantum orders. In this section, we illustrate ways in which PULSEE is deployed to put forward a novel NMR method, inspired by QIS, that allows for the engineering of pulse sequences that can effectively probe electronic correlations and tensor orders through the hyperfine interaction.

In order to explore the capabilities of PULSEE, we give a simple yet powerful illustration of two approaches to modeling the hyperfine interaction. In the first, we consider a spin-1/2 nucleus coupled to an electronic bath directly via the hyperfine interaction ($\mathcal{H}_{\rm hf} = \mathbf{S}\tilde{A}\mathbf{I}$). In the second, we examine two spin-1/2 nuclei interacting via an effective hyperfine field, $\tilde{A}$, mediated via electrons ($\mathcal{H}_{\rm hf} = \mathbf{I_1}\tilde{A}\mathbf{I_2}$). The system will be modeled as two interacting spin-1/2 particles, governed by the Hamiltonian,

$$\mathcal{H} = -\omega_n(I_z^{(1)} \otimes \mathbb{1}) + \begin{cases} -\omega_s(\mathbb{1} \otimes S_z) + \mathbf{S}\tilde{A}\mathbf{I^{(1)}}, & \text{i} \\ -\omega_n(\mathbb{1} \otimes I_z^{(2)}) + \mathbf{I^{(1)}}\tilde{A}\mathbf{I^{(2)}}, & \text{ii} \end{cases} \tag{25}$$

where I, S correspond to the nuclear/electronic spin operator, respectively. The electronic Larmor precession frequency is much greater than the nuclear precession, $\omega_s \approx 2000 \quad \omega_n$, and the Zeeman terms dominate over the hyperfine coupling.

The two forms of the hyperfine interactions are written for different applications. For instance, the Hamiltonian defined in Eq. (25)i may be useful in organic materials that exhibit very rich phase diagrams induced by strong correlations [90]. The concepts introduced in the study of open quantum systems [91] can be exploited to discern the nature of complex phases arising as a result of strong correlations. An example to consider is a target system of nuclear spins (e.g. ^{13}C) coupled to an uncontrollable electronic bath via the hyperfine interaction. The engineered auxiliary system, nuclear spins interacting via the dipole-dipole interactions, and the correlated electronic spins of the bath share an entangled state that reflects the nature of the electronic correlations we seek to identify. By simulating the form of expected experimental results, one may deploy PULSEE to devise effective pulse sequences to probe the quantum orders in such correlated phases. Furthermore, Eq. (25)i can serve as a starting point for quantum control studies [26,90,92–94].

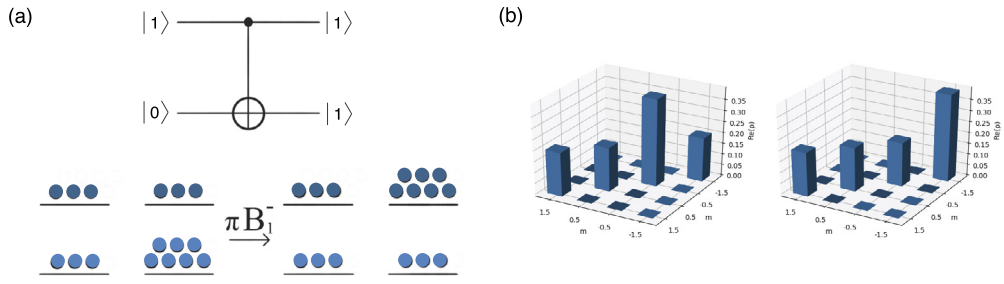

Fig. 9. (a) Symbolic notation of a CNOT gate operating on the state $|10\rangle$ (on top) and the action of the pulse which carries out the equivalent operation on the NQR version of the 2-qubit system (at the bottom). **(b)** Input (on the left) and output (on the right) states of the simulated NQR CNOT$_1$ gate when the initial state is $|10\rangle$.

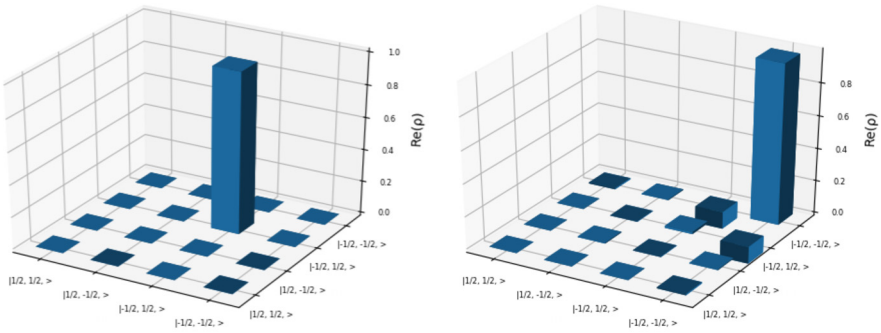

Fig. 10. Input (on the left) and output (on the right) of the simulated NMR CNOT$_1$ gate when the initial state is set to the ideal pure state $|10\rangle$. The output state presents a slight discrepancy with respect to the expected $|11\rangle$ state, which is thought to be a consequence of the discrete approximations taken in the simulation.

On the other hand, the Hamiltonian defined in Eq. (25)ii may be useful in studies of mean-field electronic correlations and in the development of the probes of tensor order [95].

Here, we demonstrate the utility of PULSEE in devising an efficient protocol to probe the nature of tensor order, *i.e.* anisotropy of the hyperfine tensor. We consider two spin-1/2 spins coupled via a hyperfine interaction of the form,

$$\tilde{A} = \begin{pmatrix} A_{aa} & 0 & A_{ac} \\ 0 & A_{aa} & 0 \\ A_{ac} & 0 & A_{aa} \end{pmatrix} \tag{26}$$

where $\tilde{A}$ is the second-rank hyperfine tensor representation for the antiferromagnetic phase (AFM) with symmetry plane $y = 0$ [96]. The diagonal terms (A_{aa}) of $\tilde{A}$ dominate, giving the principal axes. The system will be modeled as two interacting spin-1/2 particles, governed by the Hamiltonian Eq. (25)i. Working in the Zeeman-dominant regime, we investigate the evolution of the coherent spin state (CSS), as we have identified these as the most sensitive to anisotropy of the hyperfine tensor. Tuned to the nuclear spins, we can only probe the system by sending pulses to the nucleus. In the high-temperature limit, the thermal state of our system is given by

$$\rho_{\text{thermal state}} \approx \alpha \mathbb{1} - \epsilon_s S_z - \epsilon_n I_z, \tag{27}$$

where $\epsilon_s = \frac{\hbar\omega_s}{k_B T}, \epsilon_n = \frac{\hbar\omega_n}{k_B T} \sim 10^{-6} \ll 1$ are the polarization factors at room temperature T, with two different deviation density matrices for the uncorrelated electronic and nuclear spins, α is a constant that depends on the temperature and Hamiltonian of the system, and where $\hbar/k_B$ are the Planck/Boltzmann constants. We work in units of $\hbar = 1$. To obtain the CSS for the nucleus, one can transform the thermal state into a state of the form

$$\rho_{\text{CSS nucleus}} \approx \alpha \mathbb{1} - \epsilon_s \mu - \epsilon_n \sigma, \tag{28}$$

where μ is the polarized state of the electron, given by $\mu = |1\rangle\langle 1|$, whenever the electrons are in a magnetically ordered state [96], and σ is the deviation matrix of the nuclear spin's CSS. The CSS saturates the Heisenberg uncertainty relation [97] and resembles a semiclassical spin. It is of the form

$$|\zeta(\theta,\varphi)\rangle = \sum_{m=-j}^{j} \binom{2j}{j+m}^{1/2} \cos^{j+m}\frac{\theta}{2} \sin^{j-m}\frac{\theta}{2} e^{i(j-m)\varphi} |j,m\rangle\,, \tag{29}$$

where j is the nuclear spin number ($j = 1/2$, in our case), θ, φ are angles in the Bloch sphere, and $|j,m\rangle$ are the eigenstates of the I_z operator [97]. These two angles define the rotation operator $\vec{R}_{\theta\varphi} = e^{i\theta(I_x \sin\varphi - I_y \cos\varphi)}$, which is used to generate a rotated spin operator. The CSS are the eigenstates of the rotated operator, namely

$$(\vec{R}_{\theta\varphi} I_z \vec{R}^{\dagger}_{\theta\varphi}) |\zeta(\theta,\varphi)\rangle = j\,|\zeta(\theta,\varphi)\rangle\,. \tag{30}$$

The angles $\theta = \pi/2$ and $\varphi = \pi/2$ are chosen for the particular case when there is no squeezing and the squeezing parameter is unity [98,99]; thus the deviation matrix is $\sigma = |\zeta(\pi/2,\pi/2)\rangle\langle\zeta(\pi/2,\pi/2)|$. These nuclear spin coherent pseudopure states (NSCS) have been experimentally prepared using the adapted strongly modulated pulse [99]. We perform a typical FID experiment simulation to obtain the NMR spectrum by evolving the initial state under the hyperfine Hamiltonian in Eq. (25)i using the direct diagonalization method, applying a $\pi/2$ pulse to the nuclear spin, and then observing the FID. We have assumed that $B_0 = 10\,\text{T}$ and $T_2 = 50\,\mu\text{s}$ and a 20 times longer acquisition time. The hyperfine coupling is much weaker than the Zeeman term (on the order of few percent of the nuclear Zeeman term) and it creates a peak splitting proportional to A_{aa} (Fig. 11c & Fig. 12c).

We consider three different hyperfine tensors of the form depicted in Eq. (26), with $A_{ac} = 0$, $A_{ac} = \frac{1}{2}A_{aa}$, and $A_{ac} = A_{aa}$. The form of the spectra and the evolved density matrices are given in Fig. 11. Using PULSEE, we have explored the sensitivity of various nuclear spin states to the form of the hyperfine tensor. We found

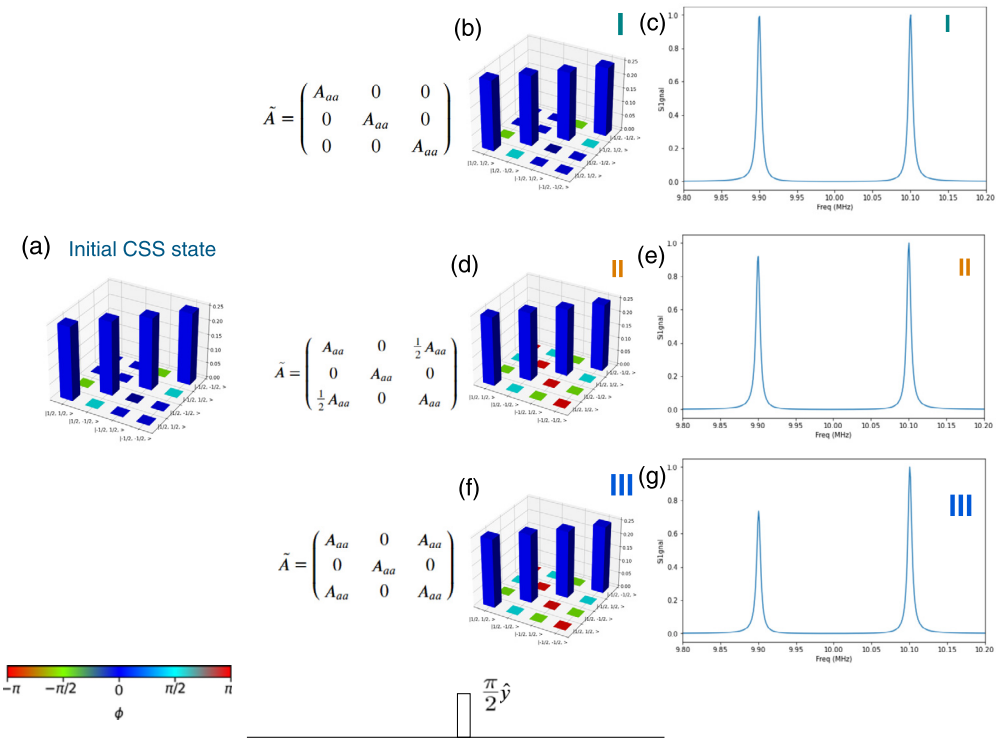

Fig. 11. Dynamics of the **(a)** coherent spin state (CSS) (Eq. (28)) in the high temperature limit. The system is evolved under the Hamiltonian (Eq. (25) i), a **(b)** $\pi/2$ pulse along I_x is applied to the nuclear spin, **(c)** observing the corresponding NMR spectrum of the FID. Three simulations are given for the three different forms of the hyperfine tensor, I fully diagonal, II off-diagonal term $A_{ac} = \frac{1}{10}A_{aa}$, and III $A_{ac} = \frac{1}{5}A_{aa}$. This CSS is sensitive to the anisotropy of the hyperfine tensor, acting as an effective probe of tensor orders.

that the particular CSS (Eq. (28)) is sensitive to the anisotropy of the hyperfine tensor. That is, the relative height of one of the peaks in the splitting changes as a function of the strength of the off-diagonal term A_{ac}. What is promising about this method is the fairly straightforward way to implement it experimentally. Once the correct CSS is prepared for the nucleus, the system is perturbed by a simple $\pi/2$ pulse along the appropriate axis, in this case I_y. Our method is similar to the spin squeezing techniques of NMR pseudo-pure states [100].

Working only with a diagonal hyperfine tensor, we show that a CNOT gate implementation (Eq. (24)) mimics the effects of the hyperfine tensor (Fig. 12). In essence, the CNOT gate introduces entanglement, where the first nuclear site is the "control qubit" and the second nuclear site is the "target qubit."

The combination of these two experiments gives us valuable information about the hyperfine tensor by studying the simple NMR spectrum. Firstly, we see that the central line of the Zeeman spectrum is split, where the splitting is given by the parameter A_{aa} of the hyperfine tensor. Furthermore, the application of the CNOT gate (Eq. (24), where the last two I_z pulses can be ignored, and $U = U(1/2A_{aa})$) suppresses one of the peaks, Fig. 12f, as expected [80,82]. Thorough investigation of the spin dynamics evolution after the application of the CNOT gate, allows us to establish the methodology for full hyperfine tensor determination.

Thus, measurements on CSS states serve as control experiments to sense the anisotropic nature of the hyperfine interaction. In other words, by performing rather manageable experiments, one may determine the nature of the hyperfine interaction, that is, the presence of off-diagonal terms, without the need of full field rotation spectroscopy [54]. Even though this simple experiment is only tuned to the nucleus, one may envision different ways to couple to the electronic spin [22,92], and then use PULSEE to investigate the dynamics of the spin and the observables.

In summary, our software allows for the simulation of complex spin evolution, which may then be used to design the appropriate pulse sequences enabling reverse engineering of the relevant Hamiltonians of tensor orders.

4.6. Building quantum circuits module: correlated density matrices

The software supports designing quantum circuits via `QubitState` objects in the `Quantum_computing` module, and tracking the dynamics of a density matrix as it evolves in the circuit. Besides being useful for quantum circuit analysis, this module is instrumental in investigating the effects of experimental artifacts, such as pulse imperfections. The effects of finite pulses applied in the laboratory cannot be equated with the those of instantaneous perfect gates. The artifacts of 'imperfect' pulses need to be considered when performing complex NMR pulse sequences. In order to evaluate the errors associated with finite pulses, one may consider the gate fidelity defined by [101]

$$F = \frac{\mathrm{Tr}(\rho_{\mathrm{th}} \cdot \rho_{\mathrm{ex}})}{\mathrm{Tr}\left(\rho_{\mathrm{th}} \cdot \rho_{\mathrm{th}}^{\dagger}\right) \mathrm{Tr}\left(\rho_{\mathrm{ex}} \cdot \rho_{\mathrm{ex}}^{\dagger}\right)}, \tag{31}$$

where ρ_{th} is the theoretical density matrix, and ρ_{ex} is the density matrix obtained experimentally through quantum tomography [102]. Using PULSEE, one may test finite pulses, determine the level of additional terms in the density matrix, and determine different pulse sequences and their fidelity in order to achieve the most adequate pulse train for the desired state evolution.

In Fig. 13 we illustrate the effect of the pulse artifacts on preparation of the nuclear spin coherent states (NSCS) using the average Hamiltonian theory method. The coherent spin state for a spin-1/2 particle whenever we use the angles $\theta = \pi/2$ and $\varphi = \pi/2$ is $|\zeta(\pi/2, \pi/2)\rangle = |+y\rangle$, or the ground eigenstate of the I_y operator. In an NMR experiment, this I_y state is obtained from a

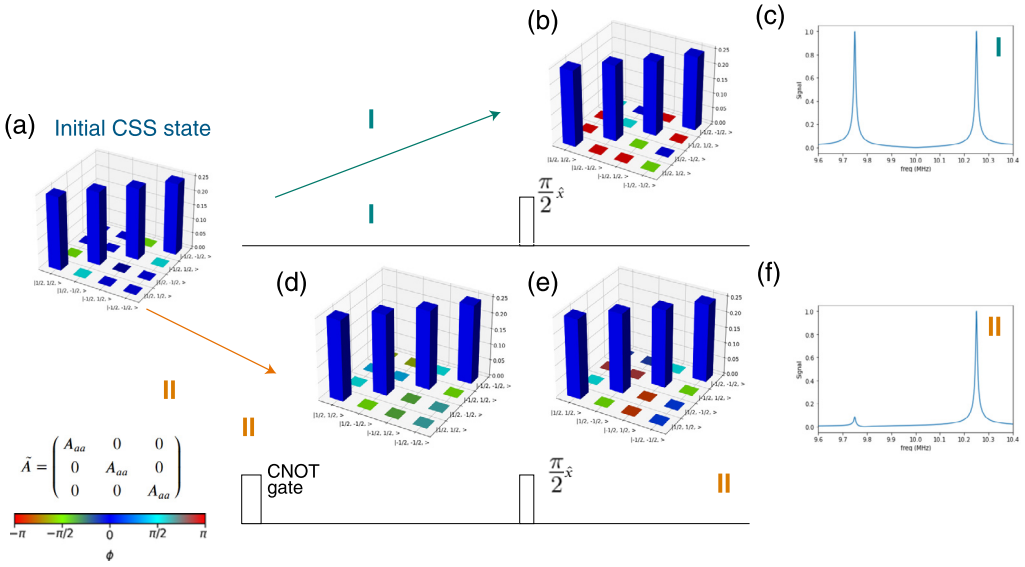

Fig. 12. Dynamics of the **(a)** coherent spin state (CSS) (Eq. (28)) in the high temperature limit. The system is evolved under the Hamiltonian (Eq. (25) i), and a **(b)** $\pi/2$ pulse along I_X is applied to the nuclear spin, **(c)** observing the corresponding NMR spectrum of the FID. The bottom row is a second experiment (**II**), where a **(d)** CNOT gate (Eq. (24)) is applied **(e)** before the $\pi/2$ pulse, **(f)** after which the FID is observed. This shows that the CNOT gate can mimic the effect of the anisotropic hyperfine tensor on the CSS.

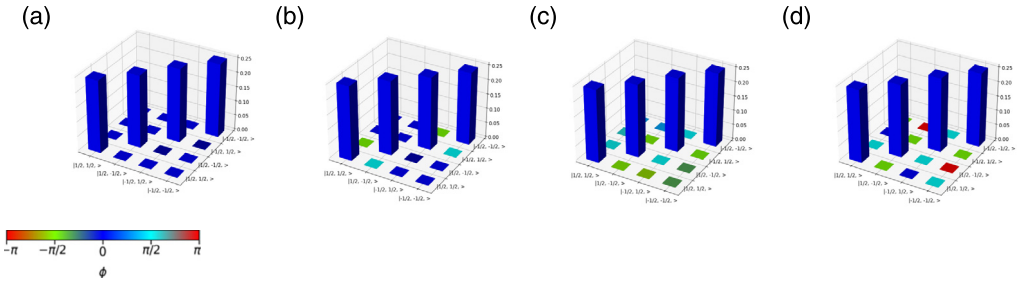

Fig. 13. Effects of the pulse artifacts on the preparation of the nuclear spin coherent states (NSCS, Eq. (28)) of a combined electronic-nuclear spin system, evolved under the second order average Hamiltonian theory mode. **(a)** Density matrix of initial thermal state (Eq. (27)) is shown for comparison, where ϕ is the phase. **(b)** Theoretical NSCS generated by instantaneous perfect pulses from Eq. (29). NSCS prepared by applying a $\pi/2$ pulse along I_x, evolved under the **(c)** Zeeman and **(d)** both Zeeman and hyperfine Hamiltonians (Eq. (25) $A_{ac} = 0$). By simulating finite NMR pulses, the evolved density matrix deviates from the theoretical one, even in the simple Zeeman case without any noise. Nevertheless, the gate fidelities (Eq. (31)) of (c, d) are nearly unity.

thermal state following the application a $\pi/2$ pulse along I_x. However, this assumes that the Hamiltonian which governs the system is a simple Zeeman one, and the $\pi/2$ pulse is perfect. We examine the effect of non-ideal $\pi/2$ pulse encountered when hyperfine interaction is present. Specifically, we simulate the effects of a non-ideal $\pi/2$ pulse by evolving the initial thermal state under two different Hamiltonians (Zeeman and hyperfine) and assume that no other noise is present in the system. Although the simulation does not include noise, we find that the density matrices differ when the full evolution of the pulse is considered under the different Hamiltonians, as depicted in Fig. 13. However, we learned that their fidelities do not notably differ from unity. These results demonstrate that, in certain experiments, one should examine the density matrices and not just consider fidelities to simulate proper time evolution of the spins.

Theoretically predicted states can be modeled using the quantum computing module as a benchmark with experimentally prepared density matrices. As an example of the quantum circuit builder, consider constructing a two-qubit, "maximally-entangled" Bell state, produced by applying a Hadamard gate to one qubit, which creates a superposition, and then subsequently applying a CNOT-gate, which entangles the two qubits by creating a control and a target qubit. The gates' matrix representations are

$$\hat{\mathrm{H}} \equiv \frac{1}{\sqrt{2}}\begin{pmatrix} 1 & 1 \\ 1 & -1 \end{pmatrix} \quad \& \quad \mathrm{CNOT} \equiv \begin{pmatrix} 1 & 0 & 0 & 0 \\ 0 & 1 & 0 & 0 \\ 0 & 0 & 0 & 1 \\ 0 & 0 & 1 & 0 \end{pmatrix}, \tag{32}$$

in the computational basis. Taking the initial state as $|00\rangle$, one obtains

$$\begin{aligned} \mathrm{CNOT}[(\hat{\mathrm{H}} \otimes \mathbb{1})\,|00\rangle] &= \mathrm{CNOT}\left[\frac{1}{\sqrt{2}}(|0\rangle + |1\rangle) \otimes |0\rangle\right] \\ &= \frac{1}{\sqrt{2}}(|00\rangle + |11\rangle), \end{aligned} \tag{33}$$

which is precisely the Bell basis state $\left|\Phi^{+}\right\rangle$. The circuit is depicted in Fig. 14**(a)**, and the density matrix produced in Fig. 14**(b)**.

Taking the control qubit as A, one may check that

$$\mathrm{Tr}\left(\rho^{A}_{|\Phi^{+}\rangle}\right) = 1/2 < 1, \tag{34}$$

confirming that this is indeed a correlated state [103].

5. Conclusions

PULSEE is an open-source software for the simulation of nuclear magnetic resonance experiments on complex materials. The main

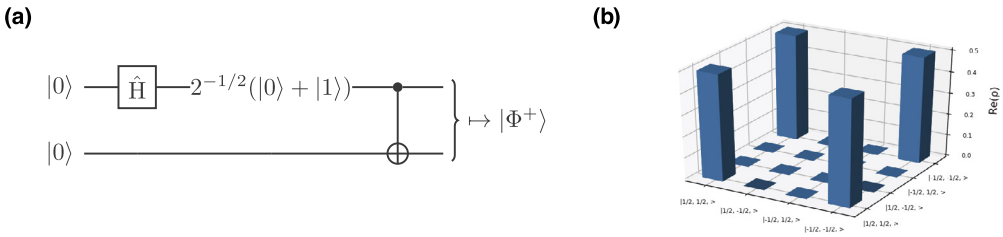

Fig. 14. **(a)** Quantum circuit diagram of the application of a Hadamard and CNOT gate to produce a Bell state from the computational basis state $|00\rangle$. **(b)** Density matrix of correlated Bell state $|\Phi_+\rangle = 2^{-1/2}(|00\rangle + |11\rangle)$.

purpose of this program is to provide a numerical tool for the development of new methods of investigation of emergent properties in complex materials inspired by the NMR/NQR protocols established in the context of quantum information processing [29].

The software follows the principles of wide accessibility and intuitive utilization as it is available for download from a public GitHub repository [52], provides a GUI, Jupyter notebooks, and a complete documentation.

The examples of execution illustrate the features of the software, including the ability to simulate both the evolution of spin states and the corresponding experimental observables, and highlight the possibilities to manipulate nuclear spin states through NMR/NQR. PULSEE enables simulations of the evolution of a single-spin under various interactions in solids. The investigation of the deviation of simulated results from experimental results on actual materials, through the subsequent inclusion of different interaction terms in the Hamiltonian, opens up an opportunity to gain valuable insight into the microscopic nature of correlations in quantum materials. In that sense, our software might find its relevance in the design of highly sensitive protocols for the study of emergent quantum properties of materials.

CRediT authorship contribution statement

Davide Candoli: Investigation, Software Programming, Development and Validation, Formal analysis, Visualization, Data curation, Writing-Original draft preparation. **Ilija K. Nikolov**: Software Programming, Development and Validation (NMR probe of Quantum correlations and quantum gates), Data curation, Writing-Original draft expansion. **Lucas Z. Brito**: Software Programming (*Quantum.computing* module), Development and Validation, Visualization, Testing. **Stephen Carr**: Software Programming, Development and Validation, Writing-Original draft expansion. **Samuele Sanna**: Methodology, Investigation, Supervision, Formal analysis, Resources, Reviewing and Editing. **Vesna F. Mitrović**: Conceptualization, Methodology, Supervision, Formal analysis, Visualization, Resources, Writing-Reviewing and Editing.

Declaration of competing interest

The authors declare the following financial interests/personal relationships which may be considered as potential competing interests: Vesna Mitrovic reports was provided by Brown University. Vesna Mitrovic reports a relationship with Brown University that includes: employment.

Data availability

Data will be made available on request.

Acknowledgements

We thank Prof. Enrico Giampieri and Prof. Sekhar Ramanathan for their helpful advice during the development of the program. We are grateful to Jonathan Frassineti for the feedback as the very first user of the program. We also thank Prof. Paolo Santini and Prof. Alessandro Chiesa for reading the manuscript and providing helpful feedback. V.F.M. acknowledges support from the U.S. National Science Foundation grants OIA-1921199 and DMR-1905532.

Appendix A. Form of different Hamiltonians

The full Hamiltonian of a single-spin nuclear system is given in Eq. (1). Here we expand on terms that are less relevant for physics, but might be useful in other disciplines, along with their secular approximations in the Zeeman dominant regime. To start, the hyperfine interaction given in Eq. (5) in the secular approximation becomes

$$\mathcal{H}_{HF} \approx AS_zI_z + BS_zI_x, \tag{A.1}$$

for $A = a_{\text{iso}} + \hbar b_D(3\cos^2\theta - 1)$, $B = 3\hbar b_D \sin\theta\cos\theta$, where a_{iso} is the Fermi contact interaction constant. The chemical shift term, $\mathcal{H}_{CS}$, describes the local structure surrounding a nucleus, and thus it is very sample-specific. Its general form is given by

$$\mathcal{H}_{CS} = -\gamma\hbar\mathbf{I}\cdot\boldsymbol{\sigma}\cdot\mathbf{B}_0, \tag{A.2}$$

where $\boldsymbol{\sigma}$ is the 3x3 chemical shift tensor. It depends on the overall electrons around the nuclear site, as well as the orientation of the sample with respect to $\mathbf{B}_0$. The chemical shift in the secular approximation is given by

$$\mathcal{H}_{CS} \approx -\gamma\hbar\sigma_{zz}(\Theta)B_0, \tag{A.3}$$

where Θ is the angle between the molecule and the applied field. The dipolar Hamiltonian $\mathcal{H}_D$ is given by

$$\mathcal{H}_D = \hbar b_D\, \mathbf{I}_1^T \cdot D \cdot \mathbf{I}_2, \tag{A.4}$$

where $b_D \equiv \frac{\mu_0\gamma_1\gamma_2\hbar}{4\pi r_{21}^3}$ is the dipolar constant, μ_0 is the magnetic constant, γ_1, γ_2 are the gyromagnetic ratio of two interacting spins, and r_{21} is the average distance between the two spins. The quantity D is the tensor that acts between the transpose of the spin operator of the first nucleus $\mathbf{I}_1^T$ and the spin operator of the second nucleus $\mathbf{I}_2$, and is given by

$$D = \begin{pmatrix} 1-3\sin^2\theta\cos^2\varphi & 3\sin^2\theta\sin\varphi\cos\varphi & 3\sin\theta\cos\theta\cos\varphi \\ 3\sin^2\theta\sin\varphi\cos\varphi & 1-3\sin^2\theta\sin^2\varphi & 3\sin\theta\cos\theta\sin\varphi \\ 3\sin\theta\cos\theta\cos\varphi & 3\sin\theta\cos\theta\sin\varphi & 1-3\cos^2\theta \end{pmatrix}, \tag{A.5}$$

where θ is the angle between the distance vector connecting the two spins and the external magnetic field $\mathbf{B}_0$, and φ is the azimuthal angle. The dipolar coupling can be approximated in the Zeeman dominant regime for the homonuclear (nuclear-nuclear) interaction, as

$$\mathcal{H}_{D1} \approx \frac{\hbar b_D}{2}\left(3\cos^2\theta - 1\right)\left[3I_{1z}I_{2z} - \mathbf{I}_1\cdot\mathbf{I}_2\right], \tag{A.6}$$

and for the heteronuclear interaction, as

$$\mathcal{H}_{D2} \approx \hbar b_D \left(3\cos^2\theta - 1\right) I_{1z} I_{2z}. \tag{A.7}$$

The J-coupling is given by

$$\mathcal{H}_J = 2\pi\hbar \mathbf{I}_1 \cdot \mathbf{J} \cdot \mathbf{I}_2, \tag{A.8}$$

where $\mathbf{J}$ is the J-coupling tensor. In the secular approximation, the J-coupling becomes

$$H_J \approx 2\pi\hbar J I_{1z} I_{2z}, \tag{A.9}$$

where the J constant is much smaller than the difference in the chemical shifts of the two sites [7].

References

[1] L.M.K. Vandersypen, I.L. Chuang, Rev. Mod. Phys. 76 (2005) 1037–1069, https://doi.org/10.1103/RevModPhys.76.1037.
[2] C. Ramanathan, N. Boulant, Z. Chen, D.G. Cory, I. Chuang, M. Steffen, Quantum Inf. Process. 3 (1) (2004) 15–44, https://doi.org/10.1007/s11128-004-3668-x.
[3] S.S. Hegde, J. Zhang, D. Suter, Phys. Rev. Lett. 124 (2020) 220501, https://doi.org/10.1103/PhysRevLett.124.220501.
[4] K. Modi, A. Brodutch, H. Cable, T. Paterek, V. Vedral, Rev. Mod. Phys. 84 (2012) 1655–1707, https://doi.org/10.1103/RevModPhys.84.1655.
[5] E.N. Kaufmann, R.J. Vianden, Rev. Mod. Phys. 51 (1979) 161–214, https://doi.org/10.1103/RevModPhys.51.161.
[6] W.P. Halperin, Rev. Mod. Phys. 58 (1986) 533–606, https://doi.org/10.1103/RevModPhys.58.533.
[7] A. Abragam, Principles of Nuclear Magnetism, Oxford University Press, 1961.
[8] R. Blinc, Phys. Rep. 79 (1981) 331, https://doi.org/10.1016/0370-1573(81)90108-3.
[9] D.G. Cory, A.F. Fahmy, T.F. Havel, Proc. Natl. Acad. Sci. USA 94 (5) (1997) 1634–1639, https://www.ncbi.nlm.nih.gov/pmc/articles/PMC19968/.
[10] I.L. Chuang, L.M.K. Vandersypen, et al., Nature 393 (1998) 143–146, https://doi.org/10.1038/30181.
[11] J.A. Jones, M. Mosca, J. Chem. Phys. 109 (5) (1998) 1648–1653, https://doi.org/10.1063/1.476739.
[12] J.A. Jones, M. Mosca, R.H. Hansen, Nature 393 (6683) (1998) 344–346, https://doi.org/10.1038/30687.
[13] L.M.K. Vandersypen, M. Steffen, G. Breyta, C.S. Yannoni, R. Cleve, I.L. Chuang, Phys. Rev. Lett. 85 (25) (2000) 5452–5455, https://doi.org/10.1103/physrevlett.85.5452.
[14] G. Long, H. Yan, Y. Li, C. Tu, J. Tao, H. Chen, M. Liu, X. Zhang, J. Luo, L. Xiao, X. Zeng, Phys. Lett. A 286 (2) (2001) 121–126, https://doi.org/10.1016/S0375-9601(01)00416-9.
[15] N. Sinha, T.S. Mahesh, K.V. Ramanathan, A. Kumar, J. Chem. Phys. 114 (10) (2001) 4415–4420, https://doi.org/10.1063/1.1346645.
[16] T.F. Havel, D.G. Cory, S. Lloyd, N. Boulant, E.M. Fortunato, M.A. Pravia, G. Teklemariam, Y.S. Weinstein, A. Bhattacharyya, J. Hou, Am. J. Phys. 70 (3) (2002) 345–362, https://doi.org/10.1119/1.1446857.
[17] T. Xin, B.-X. Wang, K.-R. Li, X.-Y. Kong, S.-J. Wei, T. Wang, D. Ruan, G.-L. Long, Chin. Phys. B 27 (2) (2018) 020308, http://stacks.iop.org/1674-1056/27/i=2/a=020308.
[18] I. Oliveira, T. Bonagamba, R. Sarthour, J. Freitas, E. de Azevedo, NMR Quantum Information Processing, Elsevier, 2007.
[19] K.R.K. Rao, T.S. Mahesh, A. Kumar, Phys. Rev. A 90 (2014) 012306, https://doi.org/10.1103/PhysRevA.90.012306.
[20] J. Teles, R. Auccaise, C. Rivera-Ascona, A.G. Araujo-Ferreira, J.P. Andreeta, T.J. Bonagamba, Quantum Inf. Process. 17 (7) (2018) 177, https://doi.org/10.1007/s11128-018-1947-1.
[21] D. Lu, K. Li, J. Li, H. Katiyar, A.J. Park, G. Feng, T. Xin, H. Li, G. Long, A. Brodutch, J. Baugh, B. Zeng, R. Laflamme, npj Quantum Inf. 3 (1) (2017) 45, https://doi.org/10.1038/s41534-017-0045-z.
[22] Y.-X. Liu, A. Ajoy, P. Cappellaro, Phys. Rev. Lett. 122 (10) (2019) 100501, https://doi.org/10.1103/PhysRevLett.122.100501.
[23] C.L. Degen, F. Reinhard, P. Cappellaro, Rev. Mod. Phys. 89 (2017) 035002, https://doi.org/10.1103/RevModPhys.89.035002.
[24] P. Cappellaro, L. Jiang, J.S. Hodges, M.D. Lukin, Phys. Rev. Lett. 102 (2009) 210502, https://doi.org/10.1103/PhysRevLett.102.210502.
[25] F. Poggiali, P. Cappellaro, N. Fabbri, Phys. Rev. X 8 (2018) 021059, https://doi.org/10.1103/PhysRevX.8.021059.
[26] H. Zhou, J. Choi, S. Choi, R. Landig, A.M. Douglas, J. Isoya, F. Jelezko, S. Onoda, H. Sumiya, P. Cappellaro, H.S. Knowles, H. Park, M.D. Lukin, Phys. Rev. X 10 (2020) 031003, https://doi.org/10.1103/PhysRevX.10.031003.
[27] P. Peng, C. Yin, X. Huang, C. Ramanathan, P. Cappellaro, Nat. Phys. 17 (4) (2021) 444–447, https://doi.org/10.1038/s41567-020-01120-z.
[28] S. Carr, I.K. Nikolov, R. Cong, A.D. Maestro, C. Ramanathan, V.F. Mitrović, Multimodal quantum spectroscopy of phase transitions with inversion symmetry, arXiv:2208.10987, https://arxiv.org/abs/2208.10987.
[29] I.K. Nikolov, S. Carr, A.G. Del Maestro, C. Ramanathan, V.F. Mitrović, Spin squeezing as a probe of emergent quantum orders, to appear in J. Phys. Soc. Jpn. Conference Proceedings LT29, arXiv:2210.03697, https://arxiv.org/abs/2210.03697.
[30] J. Johansson, P. Nation, F. Nori, Comput. Phys. Commun. 183 (8) (2012) 1760–1772.
[31] J. Johansson, P. Nation, F. Nori, Comput. Phys. Commun. 184 (4) (2013) 1234–1240, https://doi.org/10.1016/j.cpc.2012.11.019.
[32] Quantum Machines, System software company, Website, https://www.quantum-machines.co.
[33] L.V. Pourovskii, D.F. Mosca, C. Franchini, Phys. Rev. Lett. 127 (2021) 237201, https://doi.org/10.1103/PhysRevLett.127.237201.
[34] L.V. Pourovskii, S. Khmelevskyi, Proc. Natl. Acad. Sci. 118 (14) (2021), https://doi.org/10.1073/pnas.2025317118.
[35] G. Wang, C. Li, P. Cappellaro, Phys. Rev. Lett. 127 (2021) 140604, https://doi.org/10.1103/PhysRevLett.127.140604.
[36] S. Carr, C. Snider, D.E. Feldman, C. Ramanathan, J.B. Marston, V.F. Mitrović, Phys. Rev. B 106 (2022) L041119, https://journals.aps.org/prb/abstract/10.1103/PhysRevB.106.L041119.
[37] X. Turkeshi, T. Mendes-Santos, G. Giudici, M. Dalmonte, Phys. Rev. Lett. 122 (2019) 150606, https://doi.org/10.1103/PhysRevLett.122.150606.
[38] W. Zhu, Z. Huang, Y.-C. He, X. Wen, Phys. Rev. Lett. 124 (2020) 100605, https://doi.org/10.1103/PhysRevLett.124.100605.
[39] A. Allouche, G. Pouzard, Comput. Phys. Commun. 54 (1) (1989) 171–176, https://doi.org/10.1016/0010-4655(89)90042-8.
[40] M. Bak, J.T. Rasmussen, N.C. Nielsen, J. Magn. Res. 147 (2) (2000) 296–330, https://doi.org/10.1006/jmre.2000.2179.
[41] K. Eichele, Wsolids1 ver. 1.21.7, http://anorganik.uni-tuebingen.de/klaus/soft/index.php?p=wsolids1/wsolids1.
[42] H.J. Reich, Windnmr-pro, Windows program, https://www2.chem.wisc.edu/areas/reich/plt/windnmr.htm, Feb. 2002.
[43] D. Possa, A.C. Gaudio, J.C.C. Freitas, J. Magn. Res. 209 (2) (2011) 250–260.
[44] C. Bengs, M.H. Levitt, Magn. Reson. Chem. 56 (6) (2018) 374–414, https://doi.org/10.1002/mrc.4642.
[45] H. Hogben, M. Krzystyniak, G. Charnock, P. Hore, I. Kuprov, J. Magn. Res. 208 (2) (2011) 179–194, https://doi.org/10.1016/j.jmr.2010.11.008.
[46] M. Veshtort, R.G. Griffin, J. Magn. Res. 178 (2) (2006) 248–282, https://doi.org/10.1016/j.jmr.2005.07.018.
[47] PERCH Solutions Ltd., Perch NMR software, http://new.perchsolutions.com/.
[48] F.A. Perras, C.M. Widdifield, D.L. Bryce, Solid State Nucl. Magn. Reson. 45–46 (2012) 36–44, https://doi.org/10.1016/j.ssnmr.2012.05.002.
[49] Y. Binev, M.M.B. Marques, J. Aires-de Sousa, J. Chem. Inf. Model. 47 (6) (2007) 2089–2097, https://doi.org/10.1021/ci700172n.
[50] T. Claridge, J. Chem. Inf. Model. 49 (4) (2009) 1136–1137, https://doi.org/10.1021/ci900090d.
[51] C.D. Schwieters, G.M. Clore, J. Magn. Res. 149 (2) (2001) 239–244, https://doi.org/10.1006/jmre.2001.2300.
[52] D. Candoli, PULSEE (Program for the simULation of nuclear Spin Ensemble Evolution), https://github.com/vemiBGH/PULSEE, 2021.
[53] C. Snider, S. Carr, D.E. Feldman, C. Ramanathan, J.B. Marston, V.F. Mitrović, Comput. Phys. Commun. (2022), in preparation.
[54] L. Lu, M. Song, W. Liu, A.P. Reyes, P. Kuhns, H.O. Lee, I.R. Fisher, V.F. Mitrović, Nat. Commun. 8 (2017) 14407, https://doi.org/10.1038/ncomms14407.
[55] R. Cong, R. Nanguneri, B. Rubenstein, V.F. Mitrović, Phys. Rev. B 100 (2019) 245141, https://doi.org/10.1103/PhysRevB.100.245141.
[56] J. Zhang, S.S. Hegde, D. Suter, Phys. Rev. Lett. 125 (2020) 030501, https://doi.org/10.1103/PhysRevLett.125.030501.
[57] S. Blanes, F. Casas, J.A. Oteo, J. Ros, Eur. J. Phys. 31 (2010) 907–918, https://doi.org/10.1088/0143-0807/31/4/020.
[58] C.P. Slichter, Principles of Magnetic Resonance, Springer-Verlag, 1990.
[59] A. Redfield, in: J.S. Waugh (Ed.), Advances in Magnetic Resonance, in: Advances in Magnetic and Optical Resonance, vol. 1, Academic Press, 1965, pp. 1–32, https://doi.org/10.1016/B978-1-4832-3114-3.50007-6.
[60] Cohen-Tannoudji, J. Dupont-Roc, G. Grynberg, Atom-Photon Interactions: Basic Processes and Applications, Wiley, 1992.
[61] H.-P. Breuer, F. Petruccione, The Theory of Open Quantum Systems, Oxford University Press, 2007, https://doi.org/10.1093/acprof:oso/9780199213900.001.0001.
[62] P.J. Hore, J.A. Jones, S. Wimperis, NMR: The Toolkit. How Pulse Sequences Work, Oxford, 2015.
[63] M.A. McCoy, R.R. Ernst, Chem. Phys. Lett. 159 (5) (1989) 587–593, https://doi.org/10.1016/0009-2614(89)87537-2.
[64] D.-K. Yang, J.E. Atkins, C.C. Lester, D.B. Zax, Mol. Phys. 95 (5) (1998) 747–757, https://doi.org/10.1080/00268976.2011.9720930.
[65] G. Ferrand, G. Huber, M. Luong, H. Desvaux, J. Chem. Phys. 143 (9) (2015) 094201, https://doi.org/10.1063/1.4929783.

[66] A. Ajoy, B. Safvati, R. Nazaryan, J.T. Oon, B. Han, P. Raghavan, R. Nirodi, A. Aguilar, K. Liu, X. Cai, X. Lv, E. Druga, C. Ramanathan, J.A. Reimer, C.A. Meriles, D. Suter, A. Pines, Nat. Commun. 10 (1) (2019) 5160, https://doi.org/10.1038/s41467-019-13042-3.
[67] Y. Sung, A. Vepsäläinen, J. Braumüller, F. Yan, J.I.-J. Wang, M. Kjaergaard, R. Winik, P. Krantz, A. Bengtsson, A.J. Melville, B.M. Niedzielski, M.E. Schwartz, D.K. Kim, J.L. Yoder, T.P. Orlando, S. Gustavsson, W.D. Oliver, Nat. Commun. 12 (1) (2021) 967, https://doi.org/10.1038/s41467-021-21098-3.
[68] M.J. Weber, E.L. Hahn, Phys. Rev. 120 (1960) 365–375, https://doi.org/10.1103/PhysRev.120.365.
[69] Y. Lee, H. Robert, D. Lathrop, J. Magn. Res. 148 (2) (2001) 355–362, https://doi.org/10.1006/jmre.2000.2248.
[70] J. Miller, B. Suits, A. Garroway, J. Magn. Res. 151 (2) (2001) 228–234, https://doi.org/10.1006/jmre.2001.2366.
[71] T.P. Das, E.L. Hahn, Nuclear Quadrupole Resonance Spectroscopy, 1964, https://books.google.com/books?id=FEkAnQEACAAJ.
[72] D. Cory, R. Laflamme, E. Knill, L. Viola, T. Havel, N. Boulant, G. Boutis, E. Fortunato, S. Lloyd, R. Martinez, C. Negrevergne, M. Pravia, Y. Sharf, G. Teklemariam, Y. Weinstein, W. Zurek, Fortschr. Phys. 48 (9–11) (2000) 875–907, https://doi.org/10.1002/1521-3978(200009)48:9/11<875::AID-PROP875>3.0.CO;2-V.
[73] K.V.R.M. Murali, N. Sinha, T.S. Mahesh, M.H. Levitt, K.V. Ramanathan, A. Kumar, Phys. Rev. A 66 (2002) 022313, https://doi.org/10.1103/PhysRevA.66.022313.
[74] H. Kampermann, W.S. Veeman, J. Chem. Phys. 122 (21) (2005) 214108, https://doi.org/10.1063/1.1904595.
[75] R.M. Serra, I.S. Oliveira, Philos. Trans. R. Soc. A 370 (2012) 4615–4619, https://doi.org/10.1098/rsta.2012.0332.
[76] J.A. Jones, R.H. Hansen, M. Mosca, J. Magn. Res. 135 (2) (1998) 353–360, https://doi.org/10.1006/jmre.1998.1606, arXiv:quant-ph/9805070, http://arxiv.org/abs/quant-ph/9805070.
[77] M. Price, S. Somaroo, C. Tseng, J. Gore, A. Fahmy, T. Havel, D. Cory, J. Magn. Res. 140 (2) (1999) 371–378, https://doi.org/10.1006/jmre.1999.1851.
[78] K. Dorai, Arvind, A. Kumar, Phys. Rev. A 61 (2000) 042306, https://doi.org/10.1103/PhysRevA.61.042306.
[79] A. Güleç, S. Bahçeli, Acta Phys. Pol. A 107 (6) (2005) 983–989, https://doi.org/10.12693/APhysPolA.107.983.
[80] J. Teles, E.R. DeAzevedo, J.C.C. Freitas, R.S. Sarthour, I.S. Oliveira, T.J. Bonagamba, Philos. Trans. R. Soc. A, Math. Phys. Eng. Sci. 370 (1976) (2012) 4770–4793, https://doi.org/10.1098/rsta.2011.0365.
[81] Y.-P. Tan, X.-F. Nie, J. Li, H.-W. Chen, X.-Y. Zhou, X.-H. Peng, J.-F. Du, Chin. Phys. Lett. 29 (12) (2012) 127601, https://doi.org/10.1088/0256-307x/29/12/127601.
[82] J. Teles, C. Rivera-Ascona, R.S. Polli, R. Oliveira-Silva, E.L.G. Vidoto, J.P. Andreeta, T.J. Bonagamba, Quantum Inf. Process. 14 (6) (2015) 1889–1906, https://doi.org/10.1007/s11128-015-0967-3.
[83] G. Wolfowicz, J.J. Morton, in: R.K. Harris, R.L. Wasylishen (Eds.), eMagRes, John Wiley & Sons, Ltd, Chichester, UK, 2016, pp. 1515–1528, https://doi.org/10.1002/9780470034590.emrstm1521.
[84] J. Min, W. Teng, W. Blanchard John, F. Guanru, P. Xinhua, B. Dmitry, Sci. Adv. 4 (6) (2022) eaar6327, https://doi.org/10.1126/sciadv.aar6327.
[85] E. Knill, I. Chuang, R. Laflamme, Phys. Rev. A 57 (1998) 3348–3363, https://doi.org/10.1103/PhysRevA.57.3348.
[86] E.B. Fel'dman, A.N. Pyrkov, JETP Lett. 88 (6) (2008) 398–401, https://doi.org/10.1134/S0021364008180124.
[87] S.A. Gerasev, A.V. Fedorova, E.B. Fel'dman, E.I. Kuznetsova, Quantum Inf. Process. 17 (4) (2018) 72, https://doi.org/10.1007/s11128-018-1841-x, arXiv:1802.09042, http://arxiv.org/abs/1802.09042.
[88] M. Gärttner, P. Hauke, A.M. Rey, Phys. Rev. Lett. 120 (4) (2018) 040402, https://doi.org/10.1103/PhysRevLett.120.040402, arXiv:1706.01616, http://arxiv.org/abs/1706.01616.
[89] E. Garcia, R. Cong, P.C. Forino, A. Tassetti, G. Allodi, P. Tran, P.M. Woodward, C. Franchini, S. Sanna, V.F. Mitrović, arXiv:2210.05077, https://doi.org/10.1038/ncomms14407.
[90] Y. Suzuki, K. Wakamatsu, J. Ibuka, H. Oike, T. Fujii, K. Miyagawa, H. Taniguchi, K. Kanoda, Phys. Rev. X 12 (2022) 011016, https://doi.org/10.1103/PhysRevX.12.011016.
[91] F. Ticozzi, L. Viola, Quantum Sci. Technol. 2 (3) (2017) 034001, https://doi.org/10.1088/2058-9565/aa722a, arXiv:1704.01486, http://arxiv.org/abs/1704.01486.
[92] A. Ajoy, R. Nazaryan, K. Liu, X. Lv, B. Safvati, G. Wang, E. Druga, J.A. Reimer, D. Suter, C. Ramanathan, C.A. Meriles, A. Pines, Proc. Natl. Acad. Sci. 115 (42) (2018) 10576–10581, https://doi.org/10.1073/pnas.1807125115.
[93] J. Tian, S. Hong, I. Miotkowski, S. Datta, Y.P. Chen, Sci. Adv. 3 (4) (2017) e1602531, https://doi.org/10.1126/sciadv.1602531.
[94] M. Ahsan, S.A.Z. Naqvi, H. Anwer, Phys. Rev. A 105 (2022) 022428, https://doi.org/10.1103/PhysRevA.105.022428.
[95] Y. Zhang, C.A. Ryan, R. Laflamme, J. Baugh, Phys. Rev. Lett. 107 (2011) 170503, https://doi.org/10.1103/PhysRevLett.107.170503.
[96] G. Koutroulakis, M.D. Stewart, V.F. Mitrović, M. Horvatić, C. Berthier, G. Lapertot, J. Flouquet, Phys. Rev. Lett. 104 (2010) 087001, https://doi.org/10.1103/PhysRevLett.104.087001.
[97] J.M. Radcliffe, J. Phys. A, Math. Gen. 4 (3) (1971) 313–323, https://doi.org/10.1088/0305-4470/4/3/009.
[98] R. Auccaise Estrada, E.R. de Azevedo, E.I. Duzzioni, T.J. Bonagamba, M.H. Youssef Moussa, Eur. Phys. J. D 67 (6) (2013) 127, https://doi.org/10.1140/epjd/e2013-30689-1.
[99] R. Auccaise, A. Araujo-Ferreira, R. Sarthour, I. Oliveira, T. Bonagamba, I. Roditi, Phys. Rev. Lett. 114 (4) (2015) 043604, https://doi.org/10.1103/PhysRevLett.114.043604.
[100] S. Sinha, J. Emerson, N. Boulant, E.M. Fortunato, T.F. Havel, D.G. Cory, Quantum Inf. Process. 2 (6) (2003) 433–448, https://doi.org/10.1023/B:QINP.0000042202.87144.cb.
[101] E.M. Fortunato, M.A. Pravia, N. Boulant, G. Teklemariam, T.F. Havel, D.G. Cory, J. Chem. Phys. 116 (17) (2002) 7599–7606, https://doi.org/10.1063/1.1465412.
[102] A. Gaikwad, D. Rehal, A. Singh, Arvind, K. Dorai, Phys. Rev. A 97 (2) (2018) 022311, https://doi.org/10.1103/PhysRevA.97.022311.
[103] B.E. Baaquie, The Theoretical Foundations of Quantum Mechanics, Springer, New York, NY, 2013, pp. 93–113, https://doi.org/10.1007/978-1-4614-6224-8_6, Ch. Density Matrix: Entangled States.